

Pion Generalized Dipole Polarizabilities by Virtual Compton Scattering $\pi e \rightarrow \pi e \gamma$

C. Unkmeir,¹ A. Ocherashvili,² T. Fuchs,¹ M. A. Moinester,² and S. Scherer¹

¹ *Institut für Kernphysik, Johannes Gutenberg-Universität, J. J. Becher-Weg 45, D-55099 Mainz, Germany*

² *School of Physics and Astronomy, R. and B. Sackler Faculty of Exact Sciences, Tel Aviv University, 69978 Tel Aviv, Israel*

(July 3, 2001)

Abstract

We present a calculation of the cross section and the event generator of the reaction $\pi e \rightarrow \pi e \gamma$. This reaction is sensitive to the pion generalized dipole polarizabilities, namely, the longitudinal electric $\alpha_L(q^2)$, the transverse electric $\alpha_T(q^2)$, and the magnetic $\beta(q^2)$ which, in the real-photon limit, reduce to the ordinary electric and magnetic polarizabilities $\bar{\alpha}$ and $\bar{\beta}$, respectively. The calculation of the cross section is done in the framework of chiral perturbation theory at $\mathcal{O}(p^4)$. A pion VCS event generator has been written which is ready for implementation in GEANT simulation codes or for independent use.

13.60.Fz,14.40.Aq

I. INTRODUCTION

Pion electromagnetic polarizabilities are important dynamical properties, providing a window to the pion's internal structure (for an overview see, e.g., Refs. [1]). In a classical picture, polarizabilities determine the global, i.e. integral, deformation response of a composite system in static, uniform external electric and magnetic fields. As first shown in Refs. [2], a determination of hadron polarizabilities is possible via γ -hadron Compton scattering. So far, pion electric ($\bar{\alpha}$) and magnetic ($\bar{\beta}$) polarizabilities were investigated via $\gamma\pi \rightarrow \gamma\pi$ real Compton scattering (RCS). Since pion targets are unavailable, pion RCS was done using different artifices, such as high-energy pion-nucleus bremsstrahlung, $\pi^-Z \rightarrow \pi^-Z\gamma$ [3], radiative pion photoproduction off the proton $\gamma p \rightarrow \gamma\pi^+n$ [4], and the crossed-channel two-photon reaction $\gamma\gamma \rightarrow \pi\pi$ as embedded in the $e^-e^+ \rightarrow e^-e^+\pi^+\pi^-$ process [5,6] (see Fig. 1). The values of $\bar{\alpha}$ extracted from these experiments are given in Table I.

As can be seen, the results scatter substantially and have large uncertainties, and therefore, more experimental efforts are evidently needed. A new radiative pion photoproduction experiment at the Mainz Microtron MAMI has recently taken data [7], another one has been proposed at Jefferson Lab [8], an experiment investigating the inverse reaction $\pi^-p \rightarrow n\gamma\gamma$ has been proposed at TRIUMF [9], a new $\gamma\gamma \rightarrow \pi\pi$ experiment was proposed at Frascati [10], and new Primakoff (bremsstrahlung) experiments were proposed at CERN COMPASS [11].

Electromagnetic studies with virtual photons are advantageous, since the energy and the modulus of the three-momentum of the virtual photon can be varied independently. Furthermore, one also gets access to longitudinal degrees of freedom which cannot be tested by real photons. In the pion VCS reaction $\gamma^*\pi \rightarrow \gamma\pi$ with a virtual space-like initial-state photon and a real final-state photon, the so-called generalized polarizabilities (GPs) can be measured in the space-like region. Originally, such quantities were introduced in the context of nuclei [12] and have recently been reinvestigated for the nucleon in Ref. [13]. The analysis of the nucleon GPs is based on a multipole expansion in the center-of-mass frame below the pion production threshold. The first experimental results for generalized polarizabilities of the proton have been reported by the VCS collaboration at MAMI [14] and are in good agreement with the predictions of chiral perturbation theory [15].

Recently, another approach to the analysis of the VCS tensor has been performed in a completely covariant framework [16,17]. In particular, the reaction $\gamma^*\pi \rightarrow \gamma\pi$ is described in terms of three Lorentz-invariant functions, each depending on three scalar variables. In the limit of a soft final real photon, $q' \rightarrow 0$, the structure-dependent response is encoded in *three* generalized dipole polarizabilities $\alpha_L(q^2)$, $\alpha_T(q^2)$, and $\beta(q^2)$ [17]. The Fourier transforms of these functions are related to the electric polarization and magnetization induced by soft external fields [17]. In other words, the VCS generalized dipole polarizabilities allow one to access the local polarization response, whereas the RCS polarizabilities $\bar{\alpha} = \alpha_L(0) = \alpha_T(0)$ and $\bar{\beta} = \beta(0)$ only provide the integrated, i.e. global, response. Furthermore, *two* electric polarizabilities are needed to fully reconstruct the electric polarization, the longitudinal electric polarizability being related to the divergence of the induced electric polarization, and the transverse electric polarizability describing rotational displacements of charges which do not result in a modification of the charge density (such as, e.g., a rotating spherical charge distribution). On the other hand, due to the transverse character of the magnetic induction,

only one generalized magnetic dipole polarizability appears.

Motivated by the success of the nucleon VCS experiment [14], by studying the reaction

$$\pi e \rightarrow \pi e \gamma, \quad (1)$$

we attempt to get a hold of the pion VCS matrix element $\gamma^*(q) + \pi(p_i) \rightarrow \gamma(q') + \pi(p_f)$, which can then be utilized as a new experiment for a pion polarizability measurement.

For the numerical analysis of the above reaction, we make use of the results obtained in the framework of chiral perturbation theory at $\mathcal{O}(p^4)$ [16]. At this order in the momentum expansion, the generalized dipole polarizabilities display a degeneracy, $\beta(q^2) = -\alpha_L(q^2) = -\alpha_T(q^2)$ which will be lifted at $\mathcal{O}(p^6)$ and $\mathcal{O}(p^8)$, respectively.

Our work is organized as follows. In Sec. II, we briefly discuss the predictions for the generalized dipole polarizabilities as obtained in the framework of ChPT at $\mathcal{O}(p^4)$ [16]. We provide a physical interpretation of the longitudinal generalized electric dipole polarizability in terms of the induced polarization charge [17]. Section III briefly describes the kinematics and notation used. Section IV contains a discussion of the various pieces entering the cross section, whereas some general features of the cross section are discussed in Sec. V. Section VI introduces the ingredients of the event generator. In Sec. VII we discuss the sensitivity of the cross section to the polarizabilities. Section VIII contains the results for the cross section obtained after Monte Carlo integration. The present experimental status is summarized in Sec. IX. In Sec. X we summarize our results and draw some conclusions. The analytical results for the squared invariant amplitudes are given in the Appendix.

II. VIRTUAL COMPTON SCATTERING AND GENERALIZED DIPOLE POLARIZABILITIES

A new frontier for polarizability studies is the subject of VCS [14,18,19]. There are two different ways of studying this reaction in different kinematical regimes regarding the virtual photon. In the first case, the initial photon is real and the final virtual photon fragments into a Dalitz pair [20]. This corresponds to positive $q'^2 \geq 4m_e^2$ and will not be discussed here. Rather, we concentrate on the second case, where the initial virtual photon is produced in a particle scattering process, thus leading to $q^2 < 0$, and then scatters from a target to a real final-state photon. This process probes pion structure via the generalized dipole polarizabilities $\alpha_L(q^2)$, $\alpha_T(q^2)$, and $\beta_L(q^2)$ which in the real-photon limit, $q^2 \rightarrow 0$, reduce to the RCS polarizabilities $\alpha_L(0) = \alpha_T(0) = \bar{\alpha}$ and $\beta(0) = \bar{\beta}$ [16,17]. The predictions in the framework of ChPT at $\mathcal{O}(p^4)$ read [16] (see Fig. 2)

$$\begin{aligned} \alpha_L^{\pi^\pm}(q^2) &= \alpha_T^{\pi^\pm}(q^2) = -\beta^{\pi^\pm}(q^2) \\ &= \frac{e^2}{8\pi m_\pi} \left[\frac{4(2l_5^r - l_6^r)}{F_\pi^2} - \frac{q^2}{m_\pi^2} \frac{1}{(4\pi F_\pi)^2} J^{(0)'} \left(\frac{q^2}{m_\pi^2} \right) \right] \equiv \bar{\alpha} - f(q^2), \end{aligned} \quad (2)$$

$$\begin{aligned} \alpha_L^{\pi^0}(q^2) &= \alpha_T^{\pi^0}(q^2) = -\beta^{\pi^0}(q^2) \\ &= \frac{e^2}{4\pi m_\pi} \frac{1}{(4\pi F_\pi)^2} \left(1 - \frac{q^2}{m_\pi^2} \right) J^{(0)'} \left(\frac{q^2}{m_\pi^2} \right), \end{aligned} \quad (3)$$

where

$$J^{(0)'}(x) = \frac{1}{x} \left[1 - \frac{2}{x\sigma(x)} \ln \left(\frac{\sigma(x) - 1}{\sigma(x) + 1} \right) \right], \quad \sigma(x) = \sqrt{1 - \frac{4}{x}}, \quad x \leq 0. \quad (4)$$

The predictions for the charged pion RCS polarizabilities result from an old current-algebra low-energy theorem [21]

$$\bar{\alpha}_{\pi^\pm} = -\bar{\beta}_{\pi^\pm} = \frac{e^2}{4\pi m_\pi} \frac{2(2l_5^r - l_6^r)}{F_\pi^2} = (2.68 \pm 0.42) \times 10^{-43} \text{ cm}^3, \quad (5)$$

where the low-energy constants are fixed via the radiative pion decay $\pi^+ \rightarrow e^+ \nu_e \gamma$. Corrections at $\mathcal{O}(p^6)$ were shown to be 12% and 24% of the $\mathcal{O}(p^4)$ values for $\bar{\alpha}$ and $\bar{\beta}$, respectively [22]. The q^2 evolution of Eq. (2) [and also of (3)] is completely determined in terms of the pion mass m_π and the pion-decay constant $F_\pi = 92.4$ MeV.

The generalized dipole polarizability $\alpha_L(q^2)$ can be interpreted in terms of the influence of a static, uniform electric field \vec{E} on the pion charge form factor [17]. In the rest of this section we will not make use of a covariant notation. Breit frame kinematics has to be applied in the transition to the relativistic case. The presence of a static uniform electric field \vec{E} will induce an electric polarization, the divergence of which is defined as the polarization charge density,

$$\delta\rho(\vec{x}) = -\vec{\nabla} \cdot \vec{P}(\vec{x}). \quad (6)$$

The potential created by the original charge distribution in combination with the induced electric polarization will look like the one which is due to an effective charge density:

$$\rho_{\text{eff}}(\vec{x}) = \rho_0(\vec{x}) - \vec{\nabla} \cdot \vec{P}(\vec{x}), \quad (7)$$

where $\rho_0(\vec{x})$ is the charge density without external electric field. The form factor of this effective charge density is then given by

$$F(\vec{q}) = \int d^3x \exp(-i\vec{q} \cdot \vec{x}) \rho_{\text{eff}}(\vec{x}) = F_0(\vec{q}) + \Delta F(\vec{q}), \quad (8)$$

where $F_0(\vec{q})$ is the form factor of the ‘‘undistorted’’ charge distribution, and

$$\Delta F(\vec{q}) = 4\pi i\vec{q} \cdot \vec{E} \bar{\alpha}_L(\vec{q}) \quad (9)$$

is the lowest-order change in the form factor due to the external electric field.

In the above discussion we have concentrated on the polarization charge density, i.e., the divergence of the electric polarization, or, in terms of its Fourier transform, the longitudinal contribution, only. A full recovery of the polarization requires the transverse piece as well. For details, the interested reader is referred to the comprehensive discussion of Ref. [17].

III. VCS KINEMATICS AND DIFFERENTIAL CROSS SECTION

One possibility of studying the pion VCS matrix element would consist of investigating the electron scattering reaction $ep \rightarrow e'\gamma\pi^+n$ as an extension of the RCS experiment $\gamma p \rightarrow$

$\gamma\pi^+n$ [4,7]. In such a reaction, the VCS contribution is hidden as a subprocess in terms of a pion-pole diagram in the t channel. However, the initial pion is off its mass shell and thus the extraction involves an extrapolation to the unphysical region with all its ambiguities.

In the present work, we consider the pion VCS reaction $\pi(p_i) + e(k) \rightarrow \pi(p_f) + e(k') + \gamma(q', \epsilon')$ which, in principle, has the advantage of a direct access to the VCS matrix element without any extrapolation to the pion pole. Here the pion four-momenta in the initial and final states are denoted by $p_i^\mu = (E_i, \vec{p}_i)$ and $p_f^\mu = (E_f, \vec{p}_f)$, respectively. Similarly, the electron four-momentum reads $k^\mu = (E_k, \vec{k})$ [$k'^\mu = (E_{k'}, \vec{k}')$] and the final-state photon is characterized by its four-momentum $q'^\mu = (E_{q'}, \vec{q}')$ and polarization vector $\epsilon'^\mu = (\epsilon'^0, \vec{\epsilon}')$. The starting point of our discussion is the differential cross section in the convention of Ref. [23]:

$$d\sigma = \frac{m_e^2}{8E_f E_{k'} E_{q'}} \frac{1}{\sqrt{(p_i \cdot k)^2 - m_\pi^2 m_e^2}} \frac{1}{(2\pi)^5} \times |\overline{\mathcal{M}}|^2 \delta^4(p_i + k - p_f - k' - q') d^3 p_f d^3 k' d^3 q', \quad (10)$$

where the invariant amplitude \mathcal{M} contains the complete information on the dynamics of the process. As usual, the quantity $|\overline{\mathcal{M}}|^2$ indicates an average over the initial polarizations and a summation over the final ones.

The cross section is more conveniently expressed in terms of the five independent invariant variables (see Fig. 3)

$$\begin{aligned} s &= (p_i + k)^2, \\ s_1 &= (k' + q')^2, \\ s_2 &= (p_f + q')^2, \\ t_1 &= q'^2 = (k - k')^2, \\ t_2 &= r^2 = (p_i - p_f)^2. \end{aligned} \quad (11)$$

This introduces a Gram determinant [24]

$$\Delta_4 = \frac{1}{16} \begin{vmatrix} 2m_\pi^2 & s - m_\pi^2 - m_e^2 & 2m_\pi^2 - r^2 & s - s_2 + q^2 - m_e^2 \\ s - m_\pi^2 - m_e^2 & 2m_e^2 & s - s_1 + r^2 - m_\pi^2 & 2m_e^2 - q^2 \\ 2m_\pi^2 - r^2 & s - s_1 + r^2 - m_\pi^2 & 2m_\pi^2 & s - s_1 - s_2 \\ s - s_2 + q^2 - m_e^2 & 2m_e^2 - q^2 & s - s_1 - s_2 & 2m_e^2 \end{vmatrix} \quad (12)$$

into the expression for the fourfold differential cross section

$$\frac{d\sigma}{ds_1 ds_2 dq^2 dr^2} = \frac{1}{(2\pi)^5} \frac{2m_e^2}{\lambda(s, m_e^2, m_\pi^2)} \frac{\pi}{16} \frac{1}{(-\Delta_4)^{1/2}} |\overline{\mathcal{M}}|^2, \quad (13)$$

where

$$\lambda(s, m_e^2, m_\pi^2) = s^2 - 2(m_e^2 + m_\pi^2)s + (m_e^2 - m_\pi^2)^2. \quad (14)$$

The physical region is determined by the condition $\Delta_4 < 0$. In an actual experimental realization, the energy of the pion beam is fixed such that $s = m_\pi^2 + m_e^2 + 2E_i m_e$ in terms of laboratory variables. In other words, the differential cross section of Eq. (13) then only depends on four variables.

IV. CALCULATION OF THE SQUARED INVARIANT AMPLITUDE

At lowest order in the electromagnetic coupling, the total invariant amplitude of the reaction $\pi^\pm(p_i) + e^-(k) \rightarrow \pi^\pm(p_f) + e^-(k') + \gamma(q')$ can be divided into Bethe-Heitler (BH) and VCS contributions, $\mathcal{M} = \mathcal{M}_{\text{BH}} + \mathcal{M}_{\text{VCS}}$ (see Fig. 4). In the case of the BH diagrams of (a) and (b), the real photon is emitted by the final and initial electrons, respectively. The hadronic part of the corresponding amplitude is completely determined in terms of the pion electromagnetic form factor. We denote the space-like four-momentum of the virtual photon emitted by the pion transition current in the BH process by $r = p_i - p_f = q' + k' - k$. Due to the hermiticity of the electromagnetic current operator, the electromagnetic form factor is real in the space-like region [25]. Applying the Feynman rules of QED, it is straightforward to evaluate the BH amplitude.

The pion VCS amplitude is part of the VCS diagram (c) of Fig. 4. It is this contribution which contains the structure information in terms of the generalized dipole polarizabilities (and, of course, also of higher-order contributions).

According to Low's theorem [26], the irregular terms of the amplitudes \mathcal{M}_{BH} and \mathcal{M}_{VCS} behave as $1/E_{q'}$, where the singularities originate from the emission of the (soft) final photon at external lines. Gauge invariance then fixes terms of $\mathcal{O}(E_{q'}^0)$ which do not depend on the direction \hat{q}' (for a detailed discussion, see Refs. [27,28]). Model-dependent terms in \mathcal{M}_{VCS} are at least of order $E_{q'}$. In this context, the VCS amplitude is divided into generalized Born terms $\mathcal{M}_{\text{Born}}$, containing ground-state properties in terms of the electromagnetic form factor, and a residual non-Born contribution \mathcal{M}_{NB} , describing model-dependent internal structure (see Refs. [16,17,28]). In particular, the separation is performed such that both pieces are separately gauge invariant and the generalized Born terms contain all soft-photon singularities. The non-Born part is of $\mathcal{O}(E_{q'})$.

When squaring the total amplitude, the irregular terms of $|\overline{\mathcal{M}}|^2$ are of order $E_{q'}^{-2}$ and $E_{q'}^{-1}$. Such terms entirely originate from the BH part and the generalized Born terms of the VCS part. In particular, these contributions are completely known and can be expressed in terms of the electromagnetic form factor. Recall that the space-like virtual-photon four-momenta are r and q in the Bethe-Heitler and VCS contributions, respectively, and only in the limit $q' \rightarrow 0$ they coincide.

The spin-averaged squared invariant amplitude can be decomposed into three parts, a pure VCS part, a pure BH part, and the interference term between BH and VCS:

$$\begin{aligned} |\overline{\mathcal{M}}|^2 &= \frac{1}{2} \sum_{s,s',\lambda'} (\mathcal{M}_{\text{VCS}} + \mathcal{M}_{\text{BH}})(\mathcal{M}_{\text{VCS}}^* + \mathcal{M}_{\text{BH}}^*) \\ &= |\overline{\mathcal{M}_{\text{BH}}}|^2 + |\overline{\mathcal{M}_{\text{VCS}}}|^2 + \overline{\mathcal{M}_{\text{VCS}}\mathcal{M}_{\text{BH}}^* + \mathcal{M}_{\text{BH}}\mathcal{M}_{\text{VCS}}^*}. \end{aligned} \quad (15)$$

The Lorentz invariant matrix element for the BH amplitude reads

$$\mathcal{M}_{\text{BH}} = \pm \frac{ie^3}{r^2} \epsilon^{I*\mu}(q', \lambda') \left[(p_f + p_i)^\nu F(r^2) \right] L_{\mu\nu}^{\text{BH}}, \quad (16)$$

where the upper (lower) sign applies in the case of a π^+ (π^-) beam. Here, $L_{\mu\nu}^{\text{BH}}$ is nothing else but the second-rank electron Compton tensor,

$$\begin{aligned}
L_{\mu\nu}^{\text{BH}} &= \bar{u}(k', s') \left[\gamma_\mu \frac{1}{\gamma \cdot (k' + q') - m_e} \gamma_\nu + \gamma_\nu \frac{1}{\gamma \cdot (k - q') - m_e} \gamma_\mu \right] u(k, s) \\
&= \bar{u}(k', s') \left[\frac{\gamma_\mu \gamma \cdot q' + 2k'_\mu}{2k' \cdot q'} \gamma_\nu + \gamma_\nu \frac{\gamma \cdot q' \gamma_\mu - 2k_\mu}{2k \cdot q'} \right] u(k, s).
\end{aligned} \tag{17}$$

Equation (17) nicely displays the origin of the singularity for $q' \rightarrow 0$ as being due to the internal electron lines of the electron Compton scattering s - and u -channel diagrams approaching the on-shell limit. The squared matrix element decomposes into the product of a pure leptonic and a pure hadronic part, having the same overall sign for both π^+ and π^- ,

$$\begin{aligned}
|\overline{\mathcal{M}}_{\text{BH}}|^2 &= \frac{1}{2} \sum_{s, s', \lambda'} \mathcal{M}_{\text{BH}} \mathcal{M}_{\text{BH}}^* \\
&= \left[\frac{e^3 F(r^2)}{r^2} \right]^2 (p_i + p_f)^\mu (p_i + p_f)^\nu \overline{l}_{\mu\nu}^{\text{BH}},
\end{aligned} \tag{18}$$

with

$$\begin{aligned}
\overline{l}_{\mu\nu}^{\text{BH}} &= \frac{1}{2} \sum_{s, s', \lambda'} \bar{u}(k', s') \left(\frac{\epsilon'^* \cdot \gamma q' \cdot \gamma + 2\epsilon'^* \cdot k'}{2k' \cdot q'} \gamma_\mu + \gamma_\mu \frac{q' \cdot \gamma \epsilon'^* \cdot \gamma - 2\epsilon'^* \cdot k}{2k \cdot q'} \right) u(k, s) \\
&\quad \times \bar{u}(k, s) \left(\gamma_\nu \frac{q' \cdot \gamma \epsilon' \cdot \gamma + 2\epsilon' \cdot k'}{2k' \cdot q'} + \frac{\epsilon' \cdot \gamma q' \cdot \gamma - 2\epsilon' \cdot k}{2k \cdot q'} \gamma_\nu \right) u(k', s').
\end{aligned} \tag{19}$$

Since $\overline{l}_{\mu\nu}^{\text{BH}}$ is a product of a term containing the final-state photon polarization vector times another term containing its complex conjugate, the sum over the polarizations can be carried out immediately yielding the well-known result

$$\sum_{\lambda'} \epsilon'_\mu(\lambda') \epsilon'_\nu(\lambda') = -g_{\mu\nu}. \tag{20}$$

This simple version holds true only for the case of conserved quantities, i.e., quantities which vanish after replacement of the polarization vector with the corresponding photon momentum.¹ This is the case in the present situation. Contracting the electron spinors and using trace techniques according to Ref. [23], $\overline{l}_{\mu\nu}^{\text{BH}}$ can be expressed in terms of the four-momenta of the initial and final electrons k and k' , respectively, and the final-state photon four-momentum q' . Finally, using on-shell conditions for the electron, $k^2 = k'^2 = m_e^2$, we obtain

$$\begin{aligned}
\overline{l}_{\mu\nu}^{\text{BH}} &= -\frac{1}{2m_e^2 k \cdot q'} \left(2k_\mu k_\nu - q'_\mu k'_\nu - k'_\mu q'_\nu + h_{\mu\nu} + k \cdot k' g_{\mu\nu} \right) \\
&\quad + \frac{1}{2m_e^2 k' \cdot q'} \left(2k'_\mu k'_\nu + q'_\mu k_\nu + k_\mu q'_\nu + h_{\mu\nu} + k \cdot k' g_{\mu\nu} \right) \\
&\quad - \frac{1}{2m_e^2 k \cdot q' k' \cdot q'} \left[k \cdot k' \left(q'_\mu k'_\nu + k'_\mu q'_\nu - q'_\mu k_\nu - k_\mu q'_\nu - 2h_{\mu\nu} - 2m_e^2 g_{\mu\nu} \right) + 2m_e^2 q'_\mu q'_\nu \right]
\end{aligned}$$

¹For the general case, one would have to use the complete formula given, e.g., in Ref. [29].

$$\begin{aligned}
& -\frac{1}{m_e^2}g_{\mu\nu} - \frac{1}{2(k' \cdot q')^2} (q'_\mu k'_\nu + k'_\mu q'_\nu + h_{\mu\nu} + m_e^2 g_{\mu\nu}) \\
& + \frac{1}{2(k \cdot q')^2} (q'_\mu k'_\nu + k'_\mu q'_\nu - h_{\mu\nu} - m_e^2 g_{\mu\nu}),
\end{aligned} \tag{21}$$

where

$$h_{\mu\nu} = k_\mu k'_\nu + k'_\mu k_\nu + (k' \cdot q' - k \cdot k' - k \cdot q') g_{\mu\nu}. \tag{22}$$

Note that $\overline{l_{\mu\nu}^{\text{BH}}}$ is symmetric under $k \leftrightarrow -k'$ as well as under $\mu \leftrightarrow \nu$. Also $r^\mu \overline{l_{\mu\nu}^{\text{BH}}} = 0 = r^\nu \overline{l_{\mu\nu}^{\text{BH}}}$. The analytical result for the contraction of Eq. (18) is given in Eq. (A2) of the Appendix.

The VCS amplitude is obtained by contracting the pion VCS tensor with the initial virtual-photon and final real-photon polarization vectors $\epsilon_\mu = e\bar{u}\gamma_\mu u/q^2$ and ϵ'_ν , respectively,

$$\mathcal{M}_{\text{VCS}} = -\frac{ie^3}{q^2} \bar{u}(k', s') \gamma_\mu u(k, s) \epsilon'_\nu \mathcal{M}_{\text{VCS}}^{\mu\nu}. \tag{23}$$

The generalized Born terms of the pion VCS tensor contain, in addition to the s-channel and u-channel pole terms, a ‘‘contact term’’ in order to establish gauge invariance [16,17,28]

$$\mathcal{M}_{\text{Born}}^{\mu\nu} = F(q^2) \left[\frac{(2p_i + q)^\mu (2p_f + q')^\nu}{s_2 - m_\pi^2} + \frac{(2p_f - q)^\mu (2p_i - q')^\nu}{u_2 - m_\pi^2} - 2g^{\mu\nu} \right], \tag{24}$$

where $u_2 = (p_i - q')^2$. The most general form of the non-Born tensor involves three independent structures with corresponding invariant amplitudes depending on three invariant variables (see Refs. [16,17,30,31]). Here we will only consider the low-energy limit and make use of the $\mathcal{O}(p^4)$ predictions of Eq. (2). In this approximation the non-Born terms read

$$\mathcal{M}_{\text{NB}}^{\mu\nu} = -\frac{8\pi m_\pi}{e^2} (q'^\mu q^\nu - q \cdot q' g^{\mu\nu}) \alpha_L(q^2), \tag{25}$$

where $\alpha_L(q^2)$ is given in Eq. (2).

The squared pure VCS matrix element involves the standard lepton tensor known from the one-photon exchange approximation in electro-production processes,

$$\begin{aligned}
\overline{\eta}_{\mu\nu} &= \frac{1}{2} \sum_{s,s'} [\bar{u}(k', s') \gamma_\mu u(k, s)] [\bar{u}(k', s') \gamma_\nu u(k, s)]^* \\
&= \frac{1}{2m_e^2} [k'_\mu k'_\nu + k'_\mu k_\nu + g_{\mu\nu}(m_e^2 - k \cdot k')] \\
&= \frac{1}{4m_e^2} (K_\mu K_\nu - q_\mu q_\nu + q^2 g_{\mu\nu}),
\end{aligned} \tag{26}$$

where $K = k + k'$ and $q = k - k'$. The second equation is particularly useful when contracting with another ‘‘conserved’’ tensor. The lepton tensor is contracted with a hadronic tensor of the form²

²At $\mathcal{O}(p^4)$, for space-like q^2 all quantities are real, even for $s_2 \geq (3m_\pi)^2$, and we could, in principle, omit the complex conjugation. However, for the sake of generality, we stick to the full notation.

$$\overline{H_{\text{VCS}}^{\mu\nu}} = \sum_{\lambda'} \epsilon_{\rho}^{\prime*} \mathcal{M}_{\text{VCS}}^{\mu\rho} [\epsilon_{\sigma}^{\prime*} \mathcal{M}_{\text{VCS}}^{\nu\sigma}]^* = -g_{\rho\sigma} \mathcal{M}_{\text{VCS}}^{\mu\rho} \mathcal{M}_{\text{VCS}}^{\nu\sigma*}, \quad (27)$$

where, again, we made use of Eq. (20). Using Eq. (26) together with current conservation, we then obtain

$$\begin{aligned} |\overline{\mathcal{M}_{\text{VCS}}}|^2 &= \left(\frac{e^3}{q^2}\right)^2 \overline{\eta_{\mu\nu} H_{\text{VCS}}^{\mu\nu}} \\ &= -\left(\frac{e^3}{q^2}\right)^2 \frac{1}{4m_e^2} \left(K_{\mu} M_{\text{VCS}}^{\mu\rho} K^{\nu} M_{\nu\rho}^{\text{VCS}*} + q^2 M_{\text{VCS}}^{\mu\rho} M_{\mu\rho}^{\text{VCS}*}\right). \end{aligned} \quad (28)$$

Squaring the VCS tensor as in Eq. (28) gives rise to three distinct contributions. They involve, respectively, the contraction of the generalized Born terms, of the interference between the generalized Born terms and the residual terms, and of the residual terms involving the polarizabilities. The respective analytical results can be found in Eqs. (A3), (A4), and (A5) of the Appendix.

The interference term between the BH and the VCS amplitude can, again, be written as the contraction of a hadronic and a leptonic part. Since the BH amplitude changes sign under the substitution $\pi^+ \leftrightarrow \pi^-$, the interference term is sensitive to the pion charge. The upper and lower signs apply to the cases of a π^+ and a π^- beam, respectively,

$$\begin{aligned} \overline{2\text{Re}\{\mathcal{M}_{\text{VCS}}^* \mathcal{M}_{\text{BH}}\}} &= \frac{1}{2} \sum_{s,s',\lambda'} 2\text{Re}\{\mathcal{M}_{\text{VCS}}^* \mathcal{M}_{\text{BH}}\} \\ &= \pm 2 \frac{e^6}{r^2 q^2} F(r^2) (p_f + p_i)^{\nu} \overline{L_{\mu\nu\rho}^{\text{int}}} \text{Re}\{M_{\text{VCS}}^{\rho\mu*}\}, \end{aligned} \quad (29)$$

where

$$\overline{L_{\mu\nu\rho}^{\text{int}}} = \frac{1}{2} \sum_{s,s'} \bar{u}(k, s) \gamma_{\rho} u(k', s') L_{\mu\nu}^{\text{BH}}.$$

Using trace techniques one obtains

$$\begin{aligned} \overline{L_{\mu\nu\rho}^{\text{int}}} &= \frac{1}{2m_e^2} \left(\frac{1}{2k' \cdot q'} \left\{ k'_{\mu} q'_{\nu} k_{\rho} + q'_{\mu} k'_{\nu} k_{\rho} + k_{\mu} q'_{\nu} k'_{\rho} + q'_{\mu} k_{\nu} k'_{\rho} - k_{\mu} k'_{\nu} q'_{\rho} + k'_{\mu} k_{\nu} q'_{\rho} \right. \right. \\ &\quad + g_{\mu\nu} [-(m_e^2 - k \cdot k') q'_{\rho} - k' \cdot q' k_{\rho} - k \cdot q' k'_{\rho}] + g_{\mu\rho} [(m_e^2 - k \cdot k') q'_{\nu} - k' \cdot q' k_{\nu} + k \cdot q' k'_{\nu}] \\ &\quad \left. + g_{\nu\rho} [(m_e^2 - k \cdot k') q'_{\mu} + k' \cdot q' k_{\mu} - k \cdot q' k'_{\mu}] \right\} + \frac{k'_{\mu}}{k' \cdot q'} [k_{\nu} k'_{\rho} + k_{\rho} k'_{\nu} + (m_e^2 - k \cdot k') g_{\nu\rho}] \Big) \\ &\quad - \frac{1}{2m_e^2} (k \leftrightarrow -k'). \end{aligned} \quad (30)$$

Finally, the interference term can be divided into the interference of the BH part with the VCS Born and VCS non-Born contributions, respectively. The results are given in Eqs. (A7) and (A8) of the Appendix.

V. GENERAL FEATURES OF THE VCS DIFFERENTIAL CROSS SECTION

Some general features of the fourfold differential cross section, Eq. (13), can be inferred from Eqs. (A1) - (A8) of the Appendix. The s_1 dependence is dominated by the $(s_1 - m_e^2)^{-1}$ pole of the BH amplitude and the cross section varies according to this law with only a slight modification through the s_1 dependence of the VCS amplitude. The s_2 dependence is dominated by the $(s_2 - m_\pi^2)^{-1}$ pole of the VCS amplitude with modifications due to the s_2 dependence of the BH amplitude, but in this case the modification is not so small as in the case of s_1 .

The r^2 dependence is determined by the $1/(r^2)^2$ pole of the squared BH amplitude, and the q^2 dependence follows the $1/(q^2)^2$ pole behavior typical of electron scattering. The energy of the outgoing pion is expected to be high and the angle is expected to be small according to $1/(r^2)^2$ behavior of the cross section. The energy of the final-state photon is mainly expected to be low, as a consequence of the infrared divergence of the BH amplitude. The angular behavior of the final photon is determined by the $1/(s_1 - m_e^2)$ and $1/(s_2 - m_\pi^2)$ poles of the BH and VCS amplitudes, respectively. The more interesting photons related to the GPs are expected to have higher energies. The behavior of the final electron is completely determined by the $1/(q^2)^2$ behavior of the cross section.

The different behavior under the substitution $\pi^- \rightarrow \pi^+$ of \mathcal{M}_{BH} and \mathcal{M}_{VCS} ,

$$\begin{aligned}\mathcal{M}_{\text{BH}}(\pi^-) &= -\mathcal{M}_{\text{BH}}(\pi^+), \\ \mathcal{M}_{\text{VCS}}(\pi^-) &= \mathcal{M}_{\text{VCS}}(\pi^+),\end{aligned}\tag{31}$$

may be of use in identifying the contributions due to internal structure by comparing the reactions involving π^- and π^+ beams for the same kinematics [19]:

$$d\sigma(\pi^+) - d\sigma(\pi^-) \sim 4\text{Re}\{\overline{\mathcal{M}_{\text{BH}}(\pi^+)}\mathcal{M}_{\text{VCS}}^*(\pi^+)\}.\tag{32}$$

This circumstance suggests the possibility of using such a subtraction to remove from the data sample the pure BH and VCS contributions.

VI. VCS EVENT GENERATOR

The VCS event generator has been written based on the differential cross section of Eq. (13) in combination with the matrix elements of Eqs. (A2)–(A8), using three-body-final-state kinematics. The acceptance-rejection method [32] is used for event generation.

A. Generation of the invariants

The generation starts with the calculation of the squared invariant mass s associated with the incoming pion beam and the electron target [see Eq. (11)]. In terms of laboratory (lab) variables, s is given by

$$s = m_\pi^2 + m_e^2 + 2E_i m_e,\tag{33}$$

where E_i is the incident beam energy.

The VCS cross section increases rapidly if either the direction of the outgoing real photon is close to the direction of one of the outgoing charged particles (due to the $1/(s_1 - m_e^2)$ and $1/(s_2 - m_\pi^2)$ poles in the BH and VCS amplitudes, respectively), or if the energy of the outgoing real photon approaches zero (due to the infrared divergence of the $1/(s_1 - m_e^2 - q^2 + r^2)$ BH pole).

Therefore, if events are generated in the pole region, the efficiency of the acceptance-rejection method for the more interesting non-pole regions can be rather low. In order to generate interesting events at an acceptable rate, the pole regions are cut. Invariants are generated in the following regions:

$$\begin{aligned}
1000 m_e^2 &\leq s_1 \leq m_\rho^2, \\
2 m_\pi^2 &\leq s_2 \leq m_\rho^2, \\
q_{\min}^2 &< q^2 < 2m_e^2 - 2m_e E_{k'}^{\min}, \\
r_{\min}^2 &< r^2 < -2m_e E_{q'}^{\min} + q^2 + s_1 - m_e^2.
\end{aligned} \tag{34}$$

We choose $E_{k'}^{\min} = 10$ GeV in order to cut the $1/q^2$ pole and to understand the trigger acceptance. For the minimal photon energy we choose $E_{q'}^{\min} = 5$ GeV in order to cut the infrared divergence of the BH amplitude. For the generated invariants s_1 , s_2 , q^2 , and r^2 , the positivity of $-\Delta_4$ of Eq. (12) is checked. In case of a positive Δ_4 , the generated event is rejected and a new event is generated. Actually, the requirement of a negative Δ_4 is equivalent to the requirement of energy-momentum conservation. For an accepted event, both the cross section of Eq. (13) and the kinematical parameters of the outgoing particles are calculated. In Fig. 5, we show the generated distributions of events plotted with respect to the invariants of Eq. (11).

B. Calculation of energies and scattering angles of the outgoing particles

Using the definitions of Eq. (11) for the invariants, one obtains the following expressions for the energies and scattering angles of the outgoing particles with respect to the beam axis in terms of the lab variables:

$$\begin{aligned}
E_{k'} &= \frac{2m_e^2 - q^2}{2m_e}, \\
E_f &= \frac{s + r^2 - s_1 - m_\pi^2}{2m_e}, \\
E_{q'} &= \frac{s_1 + q^2 - r^2 - m_e^2}{2m_e},
\end{aligned} \tag{35}$$

and

$$\begin{aligned}
\cos(\theta_{k'}) &= \frac{s_2 - s - q^2 + m_e^2 + 2E_i E_{k'}}{2|\vec{p}_i||\vec{p}_{k'}|}, \\
\cos(\theta_{p_f}) &= \frac{r^2 - 2m_\pi^2 + 2E_i E_f}{2|\vec{p}_i||\vec{p}_f|},
\end{aligned} \tag{36}$$

$$\cos(\theta_{q'}) = \frac{q^2 - r^2 - s_2 + m_\pi^2 + 2E_i E_{q'}}{2|\vec{p}_i| E_{q'}}.$$

The distributions generated for the energies and scattering angles are shown in Figs. 6 and 7, respectively.

C. Components of the 3-momenta of the outgoing particles

We define the (x, z) plane as the horizontal plane with the beam axis in the positive z direction and the y axis directed vertically, such that \hat{e}_x , \hat{e}_y , and \hat{e}_z form a positively oriented Cartesian basis. The spherical polar components of a generic 3-momentum \vec{p} are defined as usual:

$$\begin{aligned} p_x &= |\vec{p}| \sin(\theta) \cos(\phi), \\ p_y &= |\vec{p}| \sin(\theta) \sin(\phi), \\ p_z &= |\vec{p}| \cos(\theta). \end{aligned} \tag{37}$$

The p_z components of the 3-momenta of the outgoing particles are calculated from the energies and scattering angles of the outgoing particles. To calculate the p_x and p_y components, it is necessary to know the azimuthal angles which are obtained as follows.

1. From Eq. (11),

$$s_1 = m_e^2 + 2E_{k'} E_{q'} - 2k'_x q'_x - 2k'_y q'_y - 2k'_z q'_z, \tag{38}$$

we obtain for the azimuthal angles of the final electron and photon

$$\frac{2E_{k'} E_{q'} + m_e^2 - s_1}{2k'_z q'_z} = 1 + \tan(\theta_{k'}) \tan(\theta_{q'}) \cos(\phi_{k'} + \phi_{q'}). \tag{39}$$

2. Analogously, from Eq. (11),

$$s_2 = m_\pi^2 + 2E_f E_{q'} - 2p_{f_x} q'_x - 2p_{f_y} q'_y - 2p_{f_z} q'_z, \tag{40}$$

we obtain for the azimuthal angles of the final pion and photon

$$\frac{2E_{p_f} E_{q'} + m_\pi^2 - s_2}{2p_{f_z} q'_z} = 1 + \tan(\theta_{p_f}) \tan(\theta_{q'}) \cos(\phi_{p_f} + \phi_{q'}). \tag{41}$$

We generate $\phi_{q'}$ randomly, and then use Eqs. (39) and (41) to determine ϕ_{p_f} and $\phi_{k'}$.

VII. SENSITIVITY

In Ref. [33] and in the associated bibliography, detailed descriptions are given of the different theoretical models of the pion polarizabilities. Here, we only collect the various predictions for the polarizabilities (see Table II).

For values of $\bar{\alpha}$ of the order of 10^{-42} cm³ (see Table II) one obtains for the ratio $\bar{\alpha}/(\frac{4}{3}\pi r_\pi^3) \sim 10^{-3}$, where r_π is the pion electromagnetic radius. A comparison with the hydrogen atom, for which this ratio is of the order of 1, leads to the conclusion that the pion is a very rigid object, with strong interactions between its charged constituents. As a consequence, we expect the effect of the polarizabilities on the RCS or VCS cross sections to be rather small. Therefore a crucial component of the event generation is the determination of the VCS phase space region, where the data are expected to be sensitive to the pion polarizability.

To that end, we introduce the variable *Ratio* as

$$Ratio = \frac{2\overline{Re\{\mathcal{M}_{\text{Born}}^*\mathcal{M}_{\text{NB}}\}} + 2\overline{Re\{\mathcal{M}_{\text{NB}}^*\mathcal{M}_{\text{BH}}\}} + \overline{|\mathcal{M}_{\text{NB}}|^2}}{\overline{|\mathcal{M}|^2}}. \quad (42)$$

Here, $\overline{|\mathcal{M}|^2}$ is the total squared amplitude, whereas both $\overline{Re\{\mathcal{M}_{\text{Born}}^*\mathcal{M}_{\text{NB}}\}}$ and $\overline{Re\{\mathcal{M}_{\text{NB}}^*\mathcal{M}_{\text{BH}}\}}$ depend linearly and $\overline{|\mathcal{M}_{\text{NB}}|^2}$ quadratically on the generalized dipole polarizability $\alpha_L(q^2)$ [see Eqs. (2), (A4), (A5), and (A8)]. We generated VCS events for different values of $\bar{\alpha}$ in Eq. (2). The corresponding distributions of these events with respect to the variable *Ratio* are shown in Fig. 8. For $\bar{\alpha} = 0$, we find *Ratio* values less than 0.05, due to the $f(q^2)$ term $\alpha_L(q^2)$ [see the definition of Eq. (2)]. For $\bar{\alpha} = 2.7 \times 10^{-43}$ cm³ and $\bar{\alpha} = 6.8 \times 10^{-43}$ cm³ the “sensitivity” reaches 20 % and 50 %, respectively. The q^2 -dependent term $f(q^2)$ in $\alpha_L(q^2)$ decreases relatively with increasing $\bar{\alpha}$, as shown in Fig. 9.

When

$$|Ratio| > 0.05, \quad (43)$$

the pion polarizability component of the VCS cross section exceeds 5 %. The simulation shows that this occurs only for ~ 0.1 %, ~ 0.6 %, and ~ 1.3 % of the generated events for $\bar{\alpha} = 0$, $\bar{\alpha} = 2.7$, and $\bar{\alpha} = 6.8 \times 10^{-43}$ cm³, respectively.

The differential acceptance of these polarizability-sensitive events is shown as a function of invariants in Fig. 10, from which one finds that the sensitivity of VCS to pion structure is significant in the following cases:

1. the invariant mass s_1 is larger than 0.1 GeV²,
2. the absolute value of the squared momentum transfer r^2 is larger than 0.05 GeV²,
3. the invariant mass s_2 is in the range $0.05 \text{ GeV}^2 < s_2 < 0.2 \text{ GeV}^2$.

Fig. 10 (bottom left) shows that the differential acceptance function versus q^2 is approximately flat. Therefore, the dependence of the sensitivity to the electron energy is small. Fig. 10 (bottom right) shows that the sensitivity increases with increasing absolute value of the squared momentum transfer r^2 . Therefore, the sensitivity is larger for lower values of

the outgoing pion momentum [see Fig. 11 (top)]. As a result of the infrared divergence of the BH amplitude, the sensitivity increases with increasing energy of the outgoing photon [see Fig. 11 (bottom)].

Events with $Ratio > 0.05$ are concentrated in the forward region of the angle $\theta_{\gamma\gamma}^*$ in the $e\gamma$ CM frame and in the backward region of the angle $\theta_{\gamma\gamma}^*$ of the $\pi\gamma$ CM frame, as shown in Fig. 12.

As shown by the calculations, by implementing the requirements

$$\begin{aligned} E_f &< 0.62E_i, \\ E_{q'} &> 0.15E_i, \end{aligned} \tag{44}$$

one achieves

$$SENS = \frac{\sigma_{\text{VCS}}(\bar{\alpha} = 2.7) - \sigma_{\text{VCS}}(\bar{\alpha} = 6.8)}{\sigma_{\text{VCS}}(\bar{\alpha} = 2.7)} \sim 2.25\%, \tag{45}$$

as shown in Fig. 13 (b).

However, even when there is sensitivity to $\bar{\alpha}$, the sensitivity to the q^2 dependence is very low. Fig. 14 shows the difference in the total (sensitive) cross section with and without q^2 dependence of the \mathcal{M}_{NB} amplitude Eq. (25) as a function of the beam momentum. The percentage difference is only of the order of 0.3 %.

VIII. VCS TOTAL CROSS SECTION

We have integrated the cross section of Eq. (13) for the kinematic region specified in Eq. (34) using two different Monte Carlo integration programs, namely, DIVON4 [40] and VEGAS [41]. The results are 106.7 ± 1.6 nbarn and 105.5 ± 0.26 nbarn, respectively. For further calculations, we use VEGAS, since the calculation errors given by VEGAS are about six times smaller and the calculation is twice as fast as for DIVON4. Using VEGAS, we calculate the Born cross sections of the reaction Eq. (1) and the total cross section of the process Eq. (1) for various values of $\bar{\alpha}$ including the q^2 dependence given by Eq. (25). The results are shown in Fig. 15, and the values are collected in Table III.

The small increase of the VCS total cross section for $\bar{\alpha} = 0$, with respect to the VCS-Born cross section, is due to the q^2 dependent component of the \mathcal{M}_{NB} amplitude [see Eq. (25)]. The small decrease in the VCS total cross section with increasing $\bar{\alpha}$ is due to the $\bar{\alpha}$ dependence of the \mathcal{M}_{NB} amplitude [see Eq. (25)].

We also calculated the π VCS cross section for a second kinematic region with

$$-0.2 \text{ GeV}^2 < q^2 < -0.032 \text{ GeV}^2 \tag{46}$$

for the q^2 range and ranges for s_1 , s_2 , and r^2 as given by Eq. (34). This choice corresponds to the data region studied by SELEX for Hadron-Electron elastic scattering [42]. In this region, using the VEGAS code, we find 34.7 ± 0.1 nbarn for the π VCS total cross section.

IX. EXPERIMENTAL STATUS

Pion Virtual Compton Scattering (VCS) via the reaction $\pi e \rightarrow \pi e \gamma$ was observed in the Fermilab E781 SELEX experiment [43]. SELEX used a 600 GeV π^- beam incident on target atomic electrons, detecting the incident π^- and the final state π^- , electron and γ . The number of reconstructed events and their distribution with respect to the kinematic variables (for the kinematic region studied) were shown to be in reasonable accord with the predictions. The limited statistics of the experiment did not allow deducing $\bar{\alpha}$. Ref. [43] discussed methods of improving the apparatus for a second-generation pion VCS experiment.

X. CONCLUSION

We have given explicit expressions for the differential cross section of the reaction $\pi^- e \rightarrow \pi^- e \gamma$, for which the invariant amplitude has been calculated at the one-loop level, $\mathcal{O}(p^4)$, in chiral perturbation theory. The non-Born part of the VCS amplitude depends on the generalized dipole polarizability $\alpha_L(q^2)$. In principle, there exist three generalized dipole polarizabilities which, however, are degenerate at the one-loop level. The total cross section has been calculated using Monte Carlo integration programs. With the VCS event generation we were able to identify regions of phase space which are sensitive to the pion polarizability.

ACKNOWLEDGMENTS

This work was supported by the Deutsche Forschungsgemeinschaft (SFB 201 and SFB 443), and the Israel Science Foundation founded by the Israel Academy of Sciences and Humanities.

APPENDIX A: ANALYTICAL EXPRESSIONS OF THE SQUARED INVARIANT AMPLITUDES

In this appendix we list the analytical results for the squared invariant amplitudes as obtained after contraction of the relevant tensors. The scalar products appearing naturally after contraction can be written in terms of the invariants of Eq. (11) as

$$\begin{aligned}
 K^2 &= (k + k')^2 = 4m_e^2 - q^2, \\
 P^2 &= (p_i + p_f)^2 = 4m_\pi^2 - r^2, \\
 q \cdot q' &= \frac{1}{2}(q^2 - r^2), \\
 P \cdot q &= P \cdot q' = s_2 - m_\pi^2 - \frac{1}{2}(q^2 - r^2), \\
 K \cdot q &= (k + k') \cdot (k - k') = 0, \\
 K \cdot q' &= s_1 - m_e^2 + \frac{1}{2}(q^2 - r^2),
 \end{aligned}$$

$$\begin{aligned}
K \cdot P &= 2s - s_1 - s_2 - m_\pi^2 - m_e^2 + \frac{1}{2}(q^2 + r^2) \\
2p_i \cdot K &= 2s - 2m_e^2 - s_2 + q^2 - m_\pi^2 \\
2p_f \cdot K &= 2s - 2s_1 - m_\pi^2 + r^2 - s_2 \\
u_2 - m_\pi^2 &= (p_i - q')^2 - m_\pi^2 = m_\pi^2 + q^2 - s_2 - r^2.
\end{aligned} \tag{A1}$$

The squared contributions read:

$$\begin{aligned}
\overline{|\mathcal{M}_{\text{BH}}|^2} &= - \left[\frac{e^3 F(r^2)}{r^2} \right]^2 \left[\frac{2}{(K \cdot q')^2 - (q \cdot q')^2} \right]^2 \\
&\times \left((K \cdot q')^2 (P \cdot q')^2 + (q \cdot q')^2 [P^2 r^2 + (K \cdot P)^2] + 2(K \cdot P)(P \cdot q')(K \cdot q')(q \cdot q') \right. \\
&\left. + \frac{(K \cdot q')^2 - (q \cdot q')^2}{4m_e^2} \left\{ P^2 [r^2 q^2 + (K \cdot q')^2 + (q \cdot q')^2] + r^2 [(P \cdot q')^2 + (K \cdot P)^2] \right\} \right),
\end{aligned} \tag{A2}$$

$$\begin{aligned}
\overline{|\mathcal{M}_{\text{Born}}|^2} &= - \left[\frac{e^3 F(q^2)}{q^2} \right]^2 \frac{1}{m_e^2} \left\{ \frac{m_\pi^2 [q^2 (P^2 + s_2 - u_2) + (2p_i \cdot K)^2]}{(s_2 - m_\pi^2)^2} \right. \\
&+ \frac{m_\pi^2 [q^2 (P^2 - s_2 + u_2) + (2p_f \cdot K)^2]}{(u_2 - m_\pi^2)^2} + 2q^2 + K^2 \\
&\left. + \frac{(2p_i \cdot K)(2p_f \cdot K) + P^2 q^2}{(s_2 - m_\pi^2)(u_2 - m_\pi^2)} (2m_\pi^2 - q^2) \right\},
\end{aligned} \tag{A3}$$

$$\begin{aligned}
\overline{2Re\{\mathcal{M}_{\text{Born}}\mathcal{M}_{\text{NB}}^*\}} &= - \left(\frac{e^3}{q^2} \right)^2 \left[\frac{8\pi m_\pi}{e^2} Re\{\alpha_L(q^2)\} F(q^2) \right] \frac{1}{m_e^2} \\
&\times \left\{ (p_i \cdot K p_f \cdot K + q^2 m_\pi^2) \frac{[q^2 - r^2]^2}{(s_2 - m_\pi^2)(u_2 - m_\pi^2)} \right. \\
&+ p_i \cdot K q' \cdot K \frac{u_2 - m_\pi^2 - q^2}{s_2 - m_\pi^2} - p_f \cdot K q' \cdot K \frac{s_2 - m_\pi^2 - q^2}{u_2 - m_\pi^2} \\
&\left. - \frac{1}{2} K^2 (q^2 - r^2) - (q^2)^2 \right\},
\end{aligned} \tag{A4}$$

$$\overline{|\mathcal{M}_{\text{NB}}|^2} = - \left(\frac{e^3}{q^2} \right)^2 \frac{1}{4m_e^2} \left(\frac{8\pi m_\pi}{e^2} \right)^2 |\alpha_L(q^2)|^2 [(q \cdot q')^2 K^2 + q^2 (K \cdot q')^2 + 2q^2 (q \cdot q')^2]. \tag{A5}$$

For the evaluation of the Bethe-Heitler-VCS interference term we quote an intermediate result:

$$\begin{aligned}
2P^\nu \overline{L_{\mu\nu\rho}^{\text{int}}} &= \frac{1}{m_e^2} \frac{1}{(K \cdot q')^2 - (q \cdot q')^2} \left\{ K_\rho K_\mu (P \cdot q' K \cdot q' + P \cdot K q \cdot q') - K_\rho P_\mu (K \cdot q')^2 \right. \\
&- K_\rho q_\mu P \cdot K K \cdot q' + P_\rho K_\mu q \cdot q' (q^2 - q \cdot q') - P_\rho q_\mu K \cdot q' (q^2 - q \cdot q') \\
&+ q'_\rho K_\mu P \cdot q' q \cdot q' - q'_\rho P_\mu K \cdot q' q^2 - q'_\rho q_\mu P \cdot K q \cdot q' \\
&\left. + g_{\rho\mu} [(q^2 - q \cdot q') P \cdot q' K \cdot q' + P \cdot K (q \cdot q')^2] \right\},
\end{aligned} \tag{A6}$$

where we have rewritten $k = (K + q)/2$ and $k' = (K - q)/2$, and where terms proportional to q_ρ and q'_μ have been dropped since they are contracted with the conserved VCS tensor.

The interference between the VCS Born terms and the BH terms is given by

$$\overline{2Re\{\mathcal{M}_{\text{Born}}^* \mathcal{M}_{\text{BH}}\}} = \pm \frac{e^6}{q^2 r^2} F(q^2) F(r^2) \frac{1}{m_e^2 [(K \cdot q')^2 - (q \cdot q')^2]} \times \left[\left(\frac{1}{s_2 - m_\pi^2} + \frac{1}{u_2 - m_\pi^2} \right) A + \left(\frac{1}{s_2 - m_\pi^2} - \frac{1}{u_2 - m_\pi^2} \right) B + C \right], \quad (\text{A7})$$

where

$$\begin{aligned} A &= P \cdot K q \cdot q' [(P \cdot K)^2 + P^2 q^2] \\ &\quad - K \cdot q' \{ (P^2 + q^2) (K \cdot q' P \cdot K + q^2 P \cdot q') + P \cdot q' [(K \cdot q')^2 - 2q^2 q \cdot q'] \}, \\ B &= -K \cdot q' \{ (q^2 - q \cdot q') [(P \cdot K)^2 + P^2 q^2] + P^2 (K \cdot q')^2 + P \cdot q' P \cdot K K \cdot q' \}, \\ C &= -2[K \cdot q' P \cdot q' (2q^2 - q \cdot q' + K^2) + P \cdot K q \cdot q' (q^2 + q \cdot q' + K^2) - P \cdot K (K \cdot q')^2]. \end{aligned}$$

In Eq. (A7) the upper and lower signs refer to a π^+ and a π^- beam, respectively.

Finally, the interference between the non-Born terms of the VCS amplitude and the BH terms reads

$$\overline{2Re\{\mathcal{M}_{\text{NB}}^* \mathcal{M}_{\text{BH}}\}} = \pm 8\pi m_\pi Re\{\alpha_L(q^2)\} \frac{e^4}{q^2 r^2} F(r^2) \frac{1}{m_e^2 [(K \cdot q')^2 - (q \cdot q')^2]} \times \left\{ P \cdot K [(K \cdot q')^2 (q^2 - q \cdot q') + (q \cdot q')^3 + (K^2 + q^2) (q \cdot q')^2] + P \cdot q' K \cdot q' [(K \cdot q')^2 + (q^2 - q \cdot q') (q^2 + q \cdot q') + K^2 q \cdot q'] \right\}, \quad (\text{A8})$$

where the upper and lower signs refer to a π^+ and a π^- beam, respectively. Here we made use of the approximation of Eq. (25) which is valid at $\mathcal{O}(p^4)$ in ChPT.

REFERENCES

- [1] B. R. Holstein, *Comments Nucl. Part. Phys.* **19**, 239 (1990);
A. I. L'vov, *Int. J. Mod. Phys. A* **8**, 5267 (1993);
S. Scherer, *Czech. J. Phys.* **49**, 1307 (1999);
M. A. Moinester and V. Steiner, hep-ex/9801008.
- [2] A. Klein, *Phys. Rev.* **99**, 988 (1955);
A. M. Baldin, *Nucl. Phys.* **18**, 310 (1960);
V. A. Petrun'kin, *JETP* **40**, 1148 (1961).
- [3] Yu. M. Antipov *et al.*, *Phys. Lett.* **121B**, 445 (1983);
Yu. M. Antipov *et al.*, *Z. Phys. C* **26**, 495 (1985).
- [4] T. A. Aibergenov *et al.*, *Czech. J. Phys., Sect. B* **36**, 948 (1986).
- [5] J. Boyer *et al.*, *Phys. Rev. D* **42**, 1350 (1990).
- [6] D. Babusci, S. Bellucci, G. Giordano, G. Matone, A. M. Sandorfi, and M. A. Moinester, *Phys. Lett. B* **277**, 158 (1992).
- [7] J. Ahrens *et al.*, MAMI Proposal A2/1-95 (1995);
Th. Walcher, *Measurement of the pion polarizability at MAMI*, contribution to the 3rd Workshop on Chiral Dynamics - Chiral Dynamics 2000: Theory and Experiment, Jefferson Lab, Newport News, Virginia, USA, July 17 - 22, 2000.
- [8] B. Norum and K. Wang (spokespersons), Jefferson Lab Report No. PR-00-010 (1999).
- [9] T. Gorringer (spokesman), TRIUMF Expt. E838 (1998).
- [10] G. Alexander *et al.*, *Nuovo Cim. A* **107**, 837 (1994).
- [11] M. A. Moinester, APS Town Meeting on Electromagnetic and Hadronic Physics, Newport News, Virginia, Dec 2000, hep-ex/0012063.
- [12] H. Arenhövel and D. Drechsel, *Nucl. Phys.* **A233**, 153 (1974).
- [13] P. A. M. Guichon, G. Q. Liu, and A. W. Thomas, *Nucl. Phys.* **A591**, 606 (1995).
- [14] VCS Collaboration and A1 Collaboration (J. Roche *et al.*), *Phys. Rev. Lett.* **85**, 708 (2000).
- [15] T. R. Hemmert, B. R. Holstein, G. Knöchlein, and S. Scherer, *Phys. Rev. D* **55**, 2630 (1997); *Phys. Rev. Lett.* **79**, 22 (1997).
- [16] C. Unkmeir, S. Scherer, A. I. L'vov, and D. Drechsel, *Phys. Rev. D* **61**, 034002 (2000).
- [17] A. I. L'vov, S. Scherer, B. Pasquini, C. Unkmeir, and D. Drechsel, *Phys. Rev. C* **64**, 015203 (2001).
- [18] B. R. Holstein, *Chiral Perturbation Theory and Nucleon Polarizabilities*, in Proceedings of the Workshop Chiral Dynamics: Theory and Experiment, Mainz, Germany, 1997, edited by A. M. Bernstein, D. Drechsel and Th. Walcher (Springer, Berlin, 1998).
- [19] S. Scherer, *Virtual Compton Scattering—Generalized Polarizabilities of Nucleons and Pions*, in Proceedings of the Joint ECT*/JLAB Workshop N^* Physics and Nonperturbative Quantum Chromodynamics, Trento, Italy, 1998, edited by S. Simula, B. Saghai, N. C. Mukhopadhyay, V. D. Burkert, Few-Body Systems, Supplement 11 (Springer, Wien, 1999).
- [20] A. I. L'vov, S. Scopetta, D. Drechsel, and S. Scherer, *Phys. Rev. C* **57**, 312 (1998).
- [21] M. V. Terent'ev, *Yad. Fiz.* **16**, 162 (1972) [*Sov. J. Nucl. Phys.* **16**, 87 (1973)].
- [22] U. Bürgi, *Phys. Lett. B* **377**, 147 (1996); *Nucl. Phys.* **B479**, 392 (1996).

- [23] J. D. Bjorken and S. D. Drell, *Relativistic Quantum Mechanics* (McGraw-Hill, New York, 1964).
- [24] See, e.g., E. Byckling and K. Kajantie, *Particle Kinematics* (Wiley, New York, 1973), Chap. 5.
- [25] See, e.g., F. Scheck, *Electroweak and Strong Interactions* (Springer, Berlin, 1996), Chap. 2.4.1.
- [26] F. E. Low, Phys. Rev. **110**, 974 (1958).
- [27] S. Scherer, A. Yu. Korchin, and J. H. Koch, Phys. Rev. C **54**, 904 (1996).
- [28] H. W. Fearing and S. Scherer, Few-Body Syst. **23**, 111 (1998).
- [29] See, e.g., F. Mandl and G. Shaw, *Quantum Field Theory* (Wiley, Chichester, 1984), Chap. 8.3.
- [30] D. Drechsel, G. Knöchlein, A. Metz, and S. Scherer, Phys. Rev. C **55**, 424 (1997).
- [31] D. Drechsel, G. Knöchlein, A. Yu. Korchin, A. Metz, and S. Scherer, Phys. Rev. C **57**, 941 (1998); *ibid.* **58**, 1751 (1998).
- [32] D. E. Groom *et al.* (Particle Data Group), Eur. Phys. J. C **15**, 1 (2000), Sec. 29.3.
- [33] J. Portolés and M. R. Pennington, *Theoretical Predictions for Pion Polarizabilities*, in *The Second DAΦNE Physics Handbook*, Vol. II, edited by L. Maiani, G. Pancheri, and N. Paver (INFN-Laboratori Nazionali di Frascati, Italy, 1995) p 579.
- [34] V. Bernard, B. Hiller, and W. Weise, Phys. Lett. B **205** 16 (1988);
V. Bernard und D. Vautherin, Phys. Rev. D **40**, 1615 (1989).
- [35] M. K. Volkov und A. A. Osipov, Sov. J. Nucl. Phys. **41** (1985) 659.
- [36] F. Schöberl und H. Leeb, Phys. Lett. **166B**, 355 (1986).
- [37] D. Babusci, S. Bellucci, G. Giordano, and G. Matone, Phys. Lett. B **314**, 112 (1993).
- [38] M. A. Ivanov and T. Mizutani, Phys. Rev. D **45**, 1580 (1992).
- [39] M. J. Lavelle, K. Schilcher, and N. F. Nasrallah, Phys. Lett. B **335**, 211 (1994).
- [40] DIVON4 Multidimensional Integration or Random Number Generation, CERN Program Library Short Writeups, D151.
- [41] G. P. Lepage, J. Comp. Phys. **27**, 192 (1978).
- [42] I. Eschrich et al., hep-ex/0106053.
- [43] A. Ocherashvili, Pion Virtual Compton Scattering, Ph.D. thesis, Sept. 2000, Tel Aviv University, <http://muon.tau.ac.il/~aharon/phd.html>.

TABLES

Reaction	$\bar{\alpha}$	Experiment
$\pi^- Z \rightarrow \pi^- Z \gamma$	$6.8 \pm 1.4 \pm 1.2$	Serpukov [3]
$\gamma p \rightarrow \gamma \pi^+ n$	20 ± 12	Lebedev [4]
$\gamma \gamma \rightarrow \pi^+ \pi^-$	2.2 ± 1.6	MARK-2 [5]

TABLE I. Experimental values of $\bar{\alpha}$ in units of 10^{-43} cm^3 .

Theoretical model	$\bar{\alpha}$	$\bar{\beta}$
Chiral quark model [35]	8.0	-7.8
Nonrelativistic quark model [36]	0.05	-
NJL model [34]	10.5 - 12.5	-(10.3 - 11.8)
ChPT [$\mathcal{O}(p^4)$] [1,37]	2.68 ± 0.42	$-(2.68 - 2.61) \pm 0.42$
ChPT [$\mathcal{O}(p^6)$] [22]	2.4 ± 0.5	-2.1 ± 0.5
Quark confinement model [38]	3.63	-3.41
QCD sum rules [39]	5.6 ± 0.5	-

TABLE II. Theoretical predictions of the polarizabilities in units of 10^{-43} cm^3 .

	Total cross section (nb)	Error (nb)
Born	105.2	0.25
$\bar{\alpha}=0.0$	105.9	0.26
$\bar{\alpha}=2.7$	105.5	0.26
$\bar{\alpha}=6.8$	105.3	0.25

TABLE III. Born and total cross sections of the reaction Eq. (1) for a negative pion as a function of $\bar{\alpha}$ ($\bar{\alpha}$ is given in units of 10^{-43} cm^3).

FIGURES

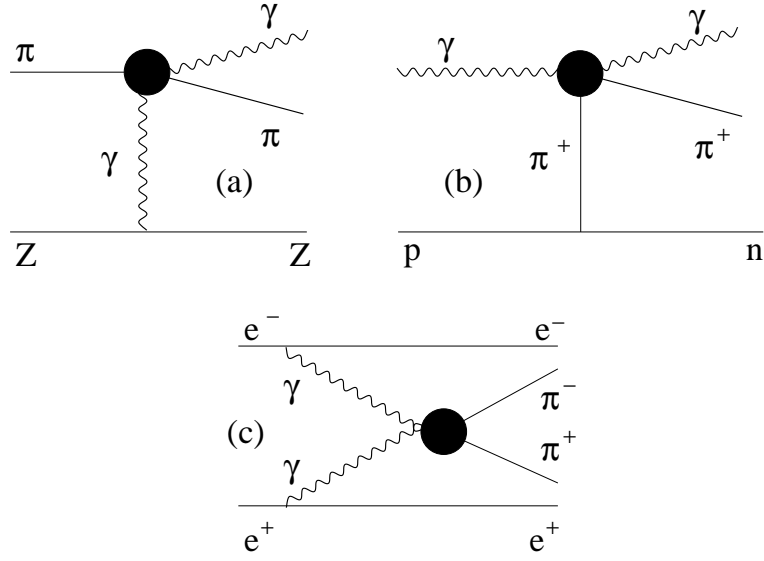


FIG. 1. Three pion Compton scattering reactions: (a) $\pi^- Z \rightarrow \pi^- Z \gamma$, (b) $\gamma p \rightarrow \gamma \pi^+ n$, (c) $e^+ e^- \rightarrow e^+ e^- \pi^+ \pi^-$.

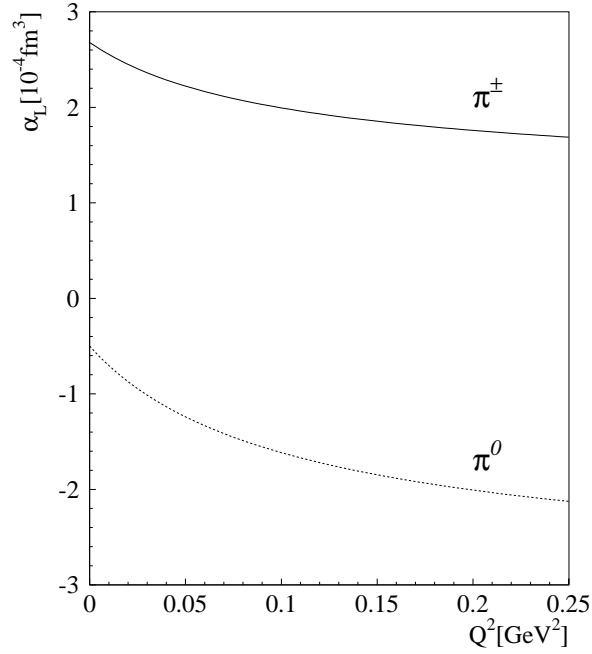


FIG. 2. $\mathcal{O}(p^4)$ prediction for the generalized dipole polarizabilities $\alpha_L(-Q^2)$ of the charged pion (solid curve) and the neutral pion (dashed curve) as functions of Q^2 [see Eqs. (2) and (3)].

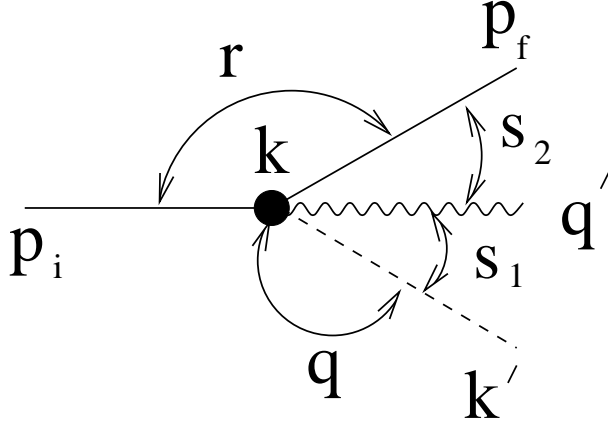


FIG. 3. Kinematics of $\pi(p_i) + e(k) \rightarrow \pi(p_f) + e(k') + \gamma(q')$ in the laboratory (lab) frame.

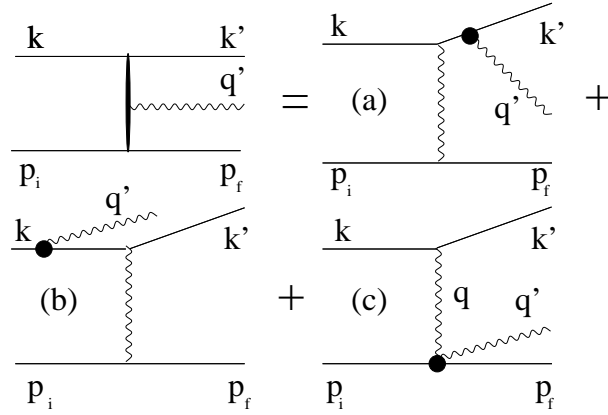


FIG. 4. The reaction $\pi^\pm(p_i) + e^-(k) \rightarrow \pi^\pm(p_f) + e^-(k') + \gamma(q')$ to lowest order in the electromagnetic coupling: Bethe-Heitler diagrams (a) and (b), VCS diagram (c). The four-momentum of the virtual photon emitted by the pion in the BH process is $r = p_i - p_f$. The four-momentum of the virtual photon absorbed in the pion VCS diagram is $q = k - k'$. Due to four-momentum conservation $r = q' - q$.

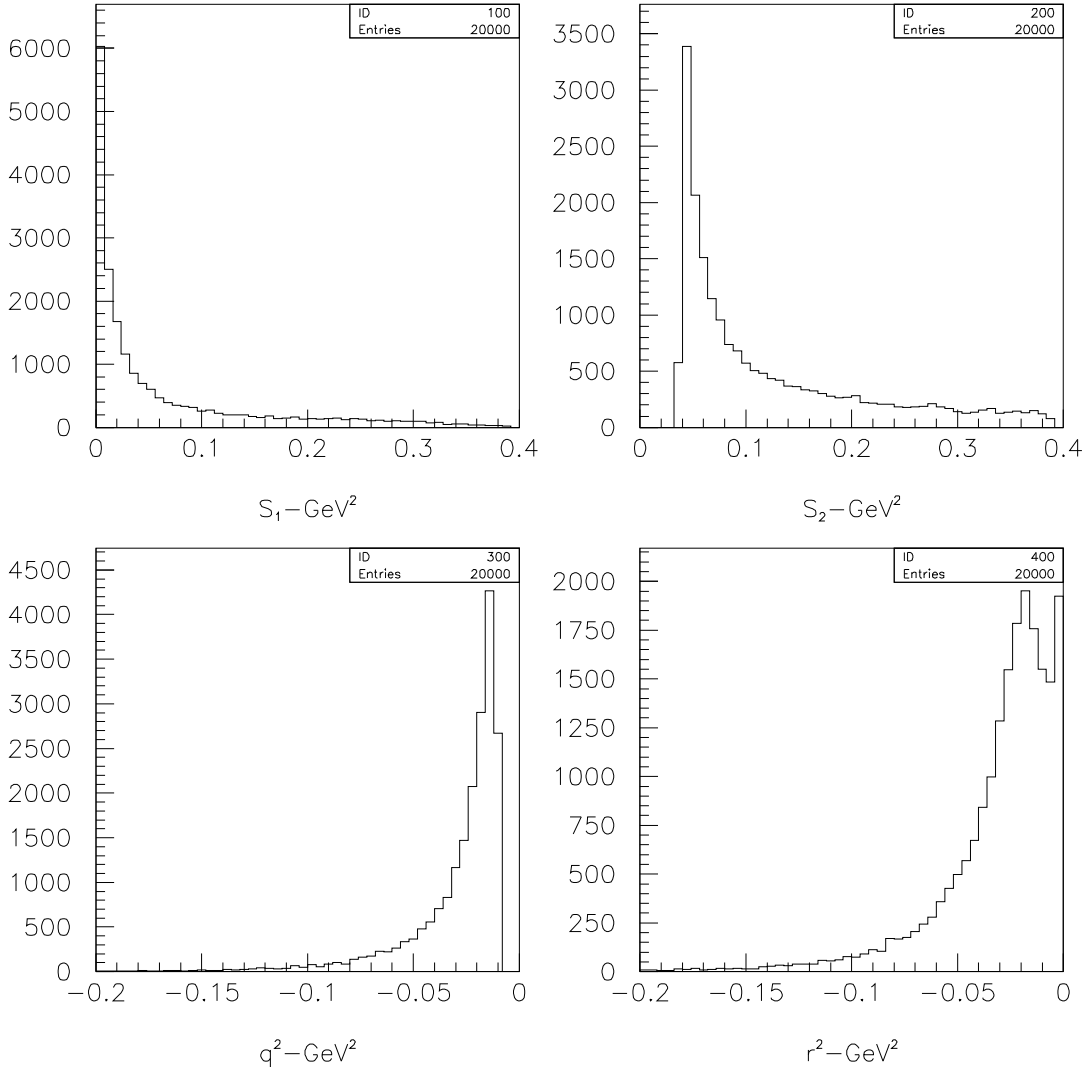


FIG. 5. Generated distributions of events plotted with respect to the invariants of Eq. (11). The generation was done with a π^- beam momentum of 650 GeV/c and $\bar{\alpha} = 6.8 \times 10^{-43} \text{ cm}^3$.

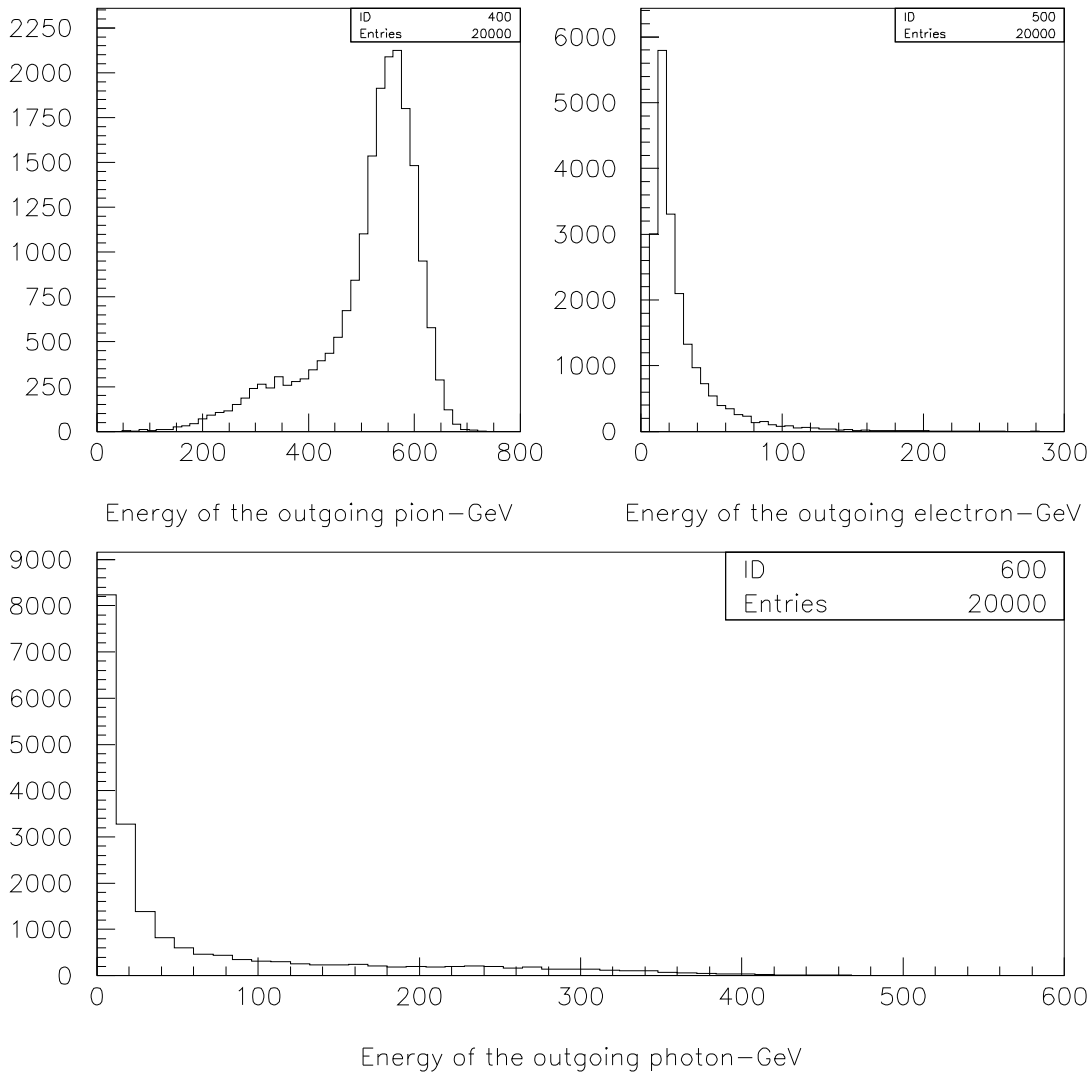


FIG. 6. Generated distributions of the energies of the final-state particles. The generation was done with a π^- beam momentum of 650 GeV/c and $\bar{\alpha} = 6.8 \times 10^{-43} \text{ cm}^3$.

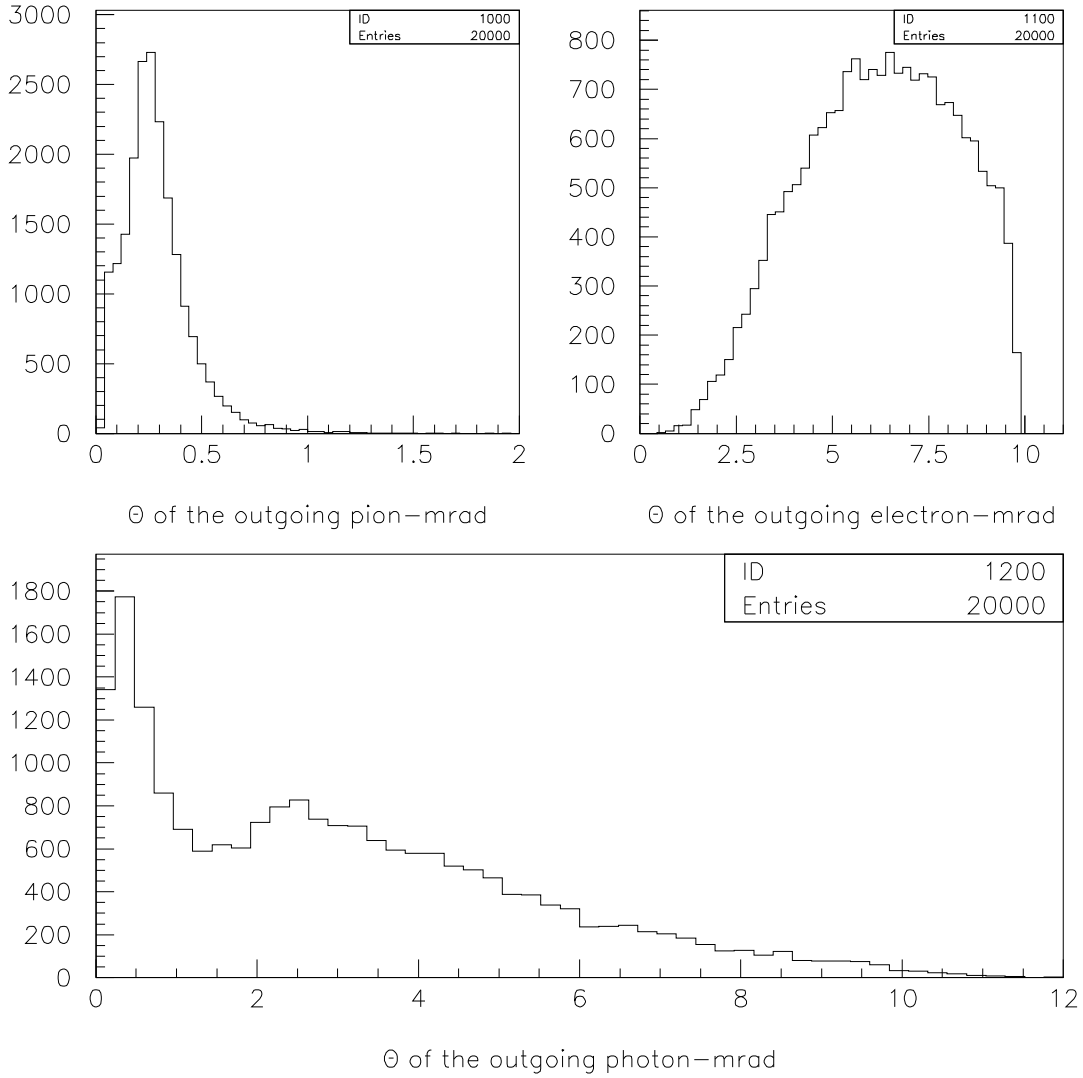


FIG. 7. Generated distributions of the θ scattering angles of the final-state particles. The generation was done with a π^- beam momentum of 650 GeV/c and $\bar{\alpha} = 6.8 \times 10^{-43} \text{ cm}^3$.

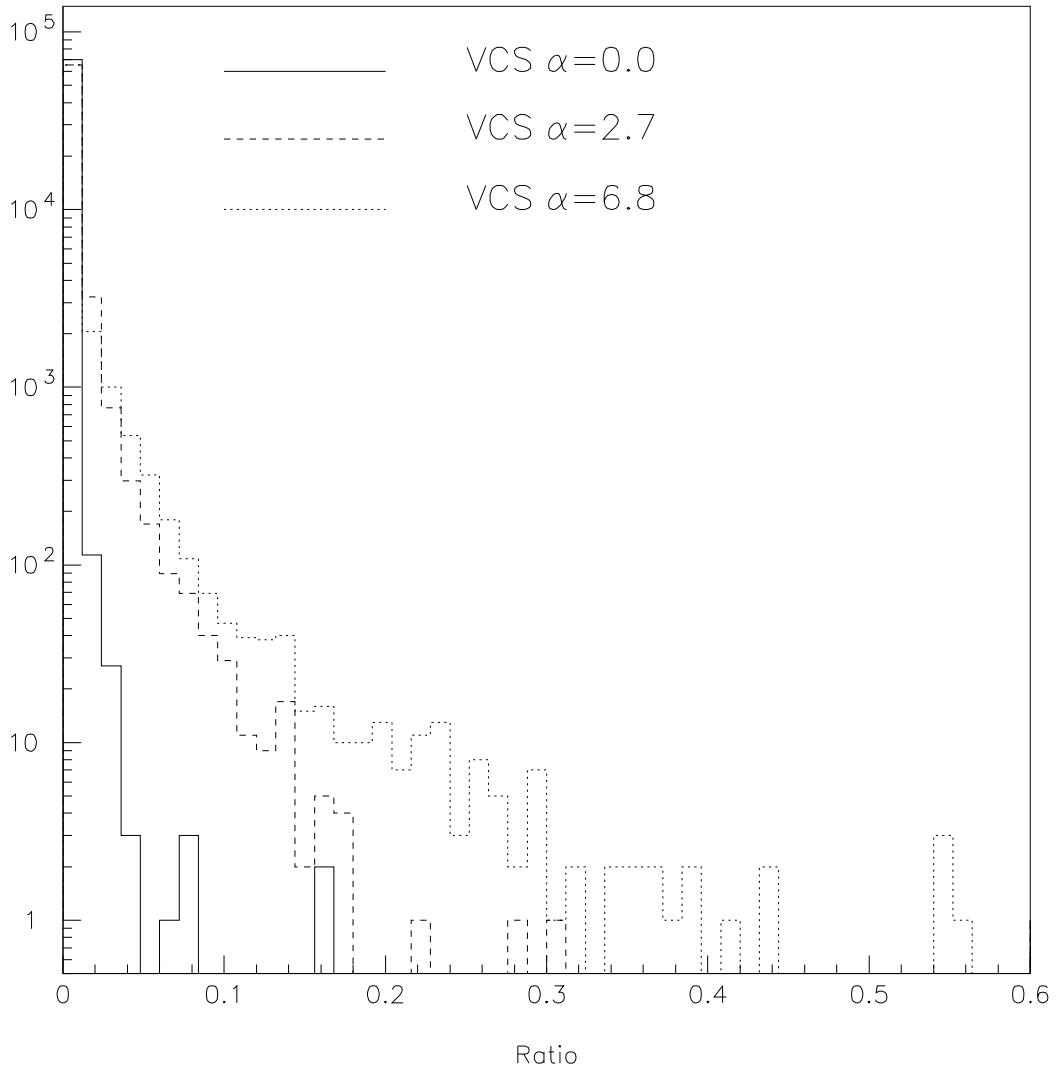


FIG. 8. The distributions of the variable *Ratio* [see Eq. (42)] for different values of the pion polarizability.

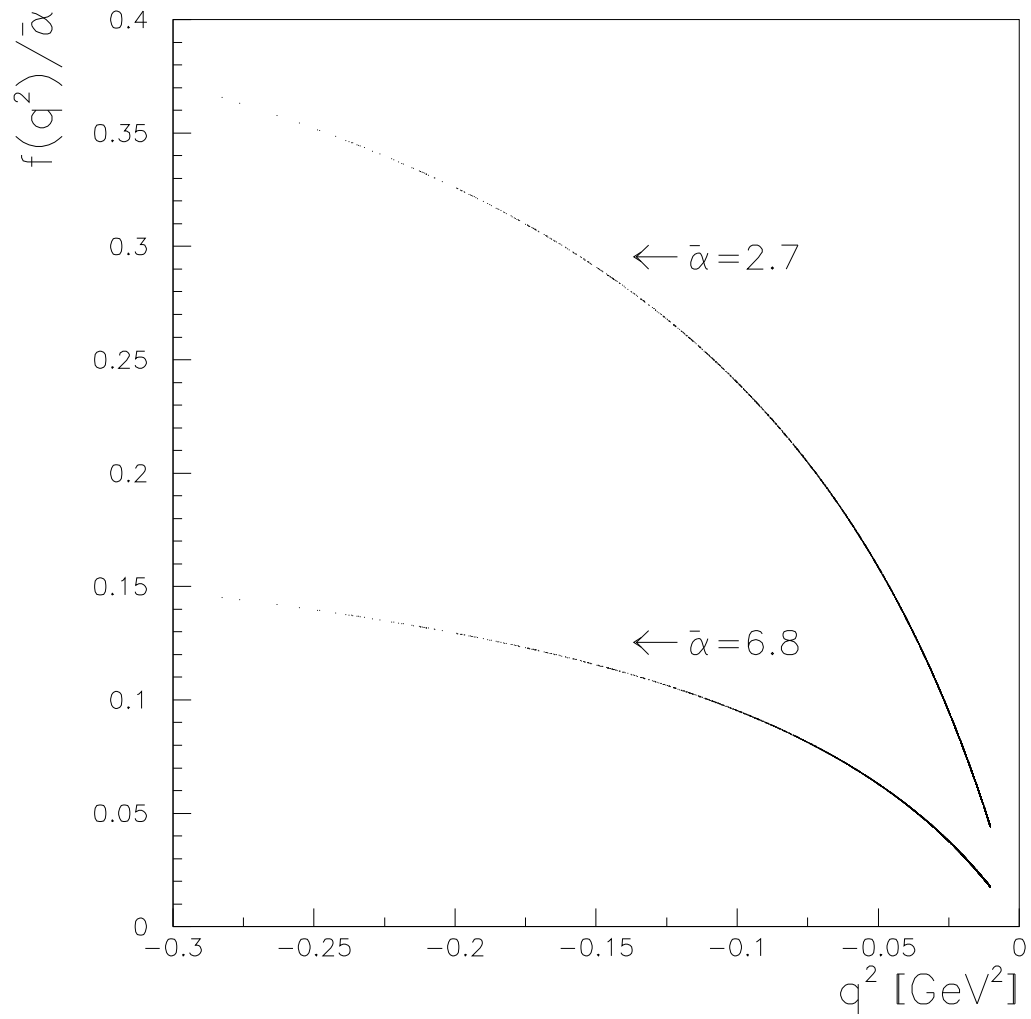


FIG. 9. Plot of $f(q^2)/(\bar{\alpha})$ (Eq. (2)) versus q^2 , for $\bar{\alpha} = 2.7 \times 10^{-43}$ and $\bar{\alpha} = 6.8 \times 10^{-43}$.

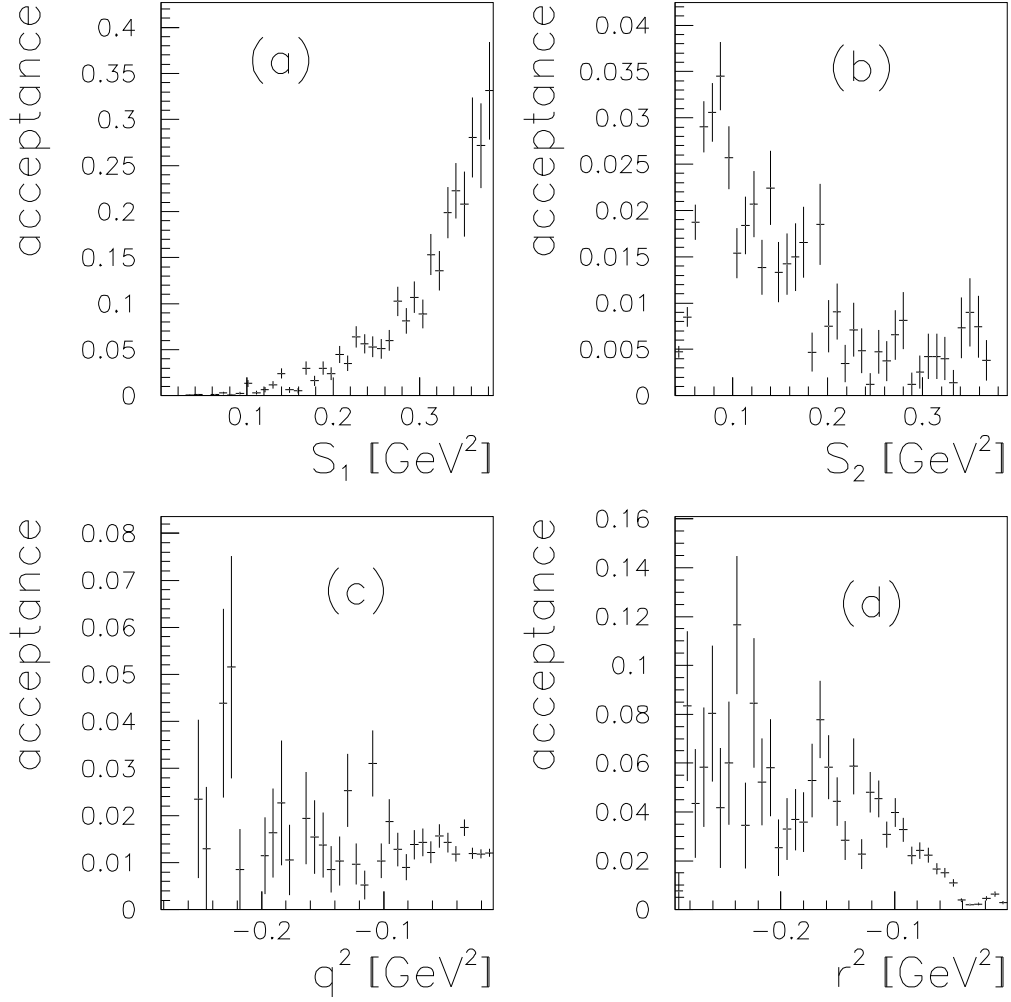


FIG. 10. The differential acceptance function of events that satisfy the condition of Eq. (43) for the invariants for $\bar{\alpha} = 6.8 \times 10^{-43} \text{ cm}^3$.

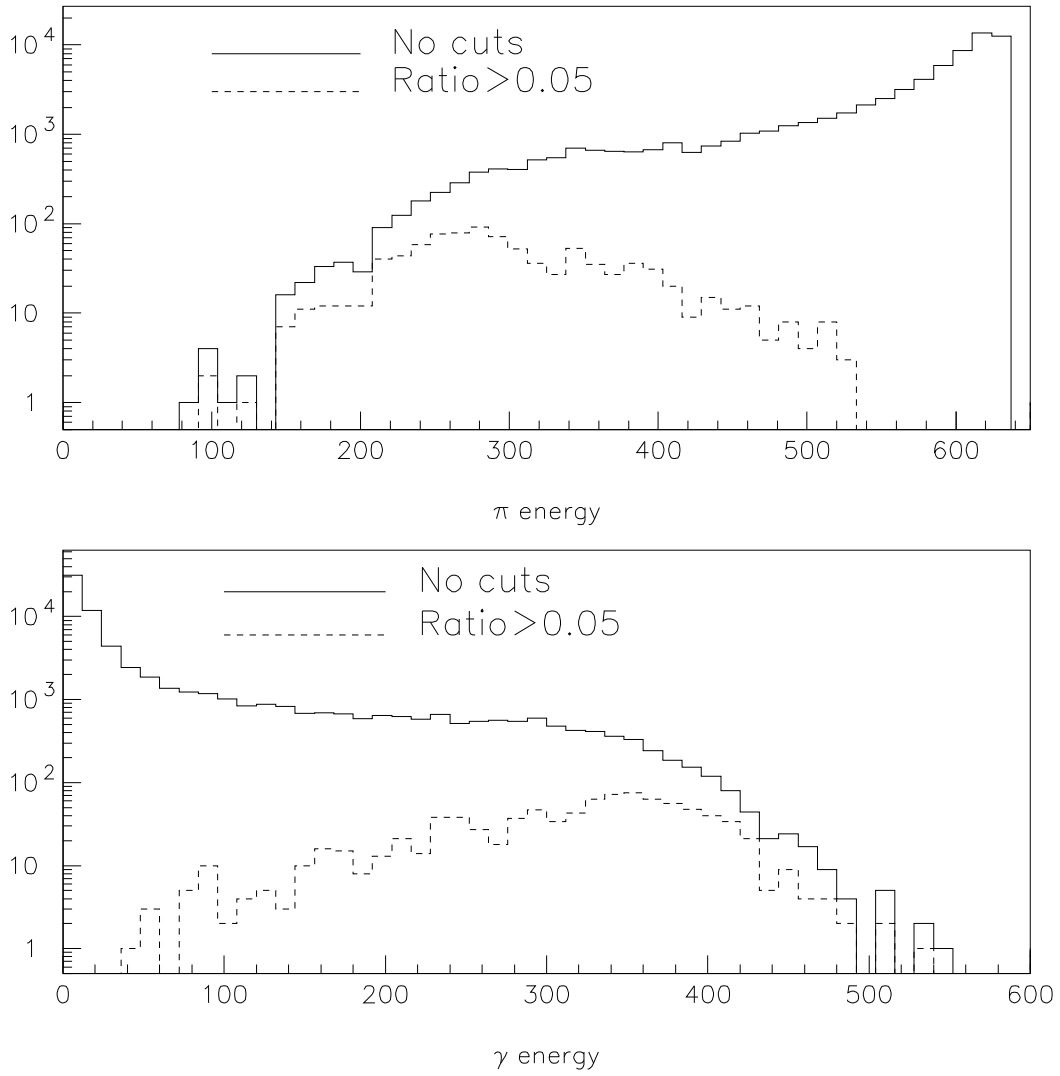


FIG. 11. The generated distribution of the energy of the pion (top) and the photon (bottom). The dashed line shows the part of the distribution with $Ratio > 0.05$ [see Eq. (43)].

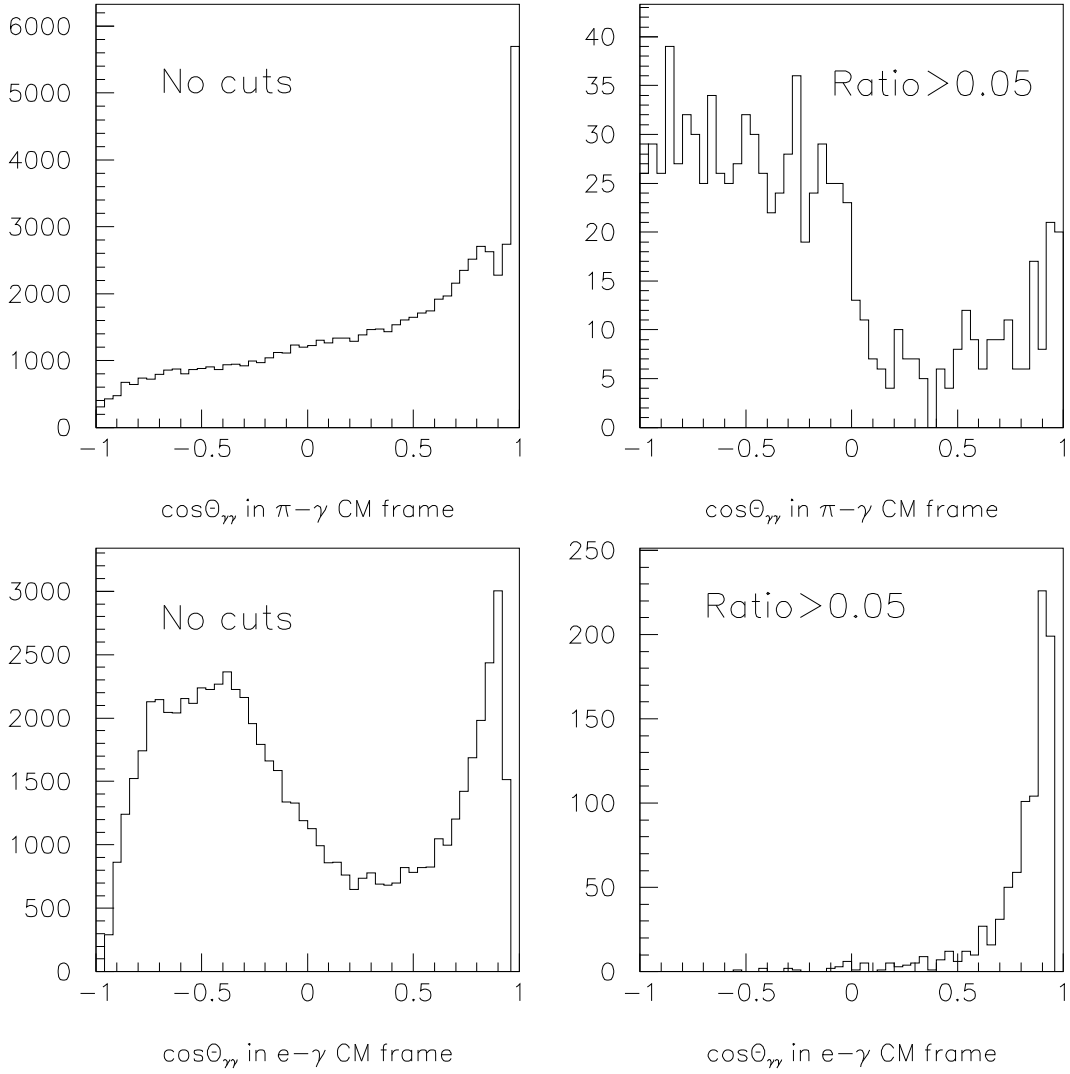


FIG. 12. The generated distribution of the angle $\theta_{\gamma\gamma}^*$ in the $\pi\gamma$ (top) and $e\gamma$ (bottom) CM frames, respectively. Distributions with $Ratio > 0.05$ [see Eq. (43)] are shown on the right.

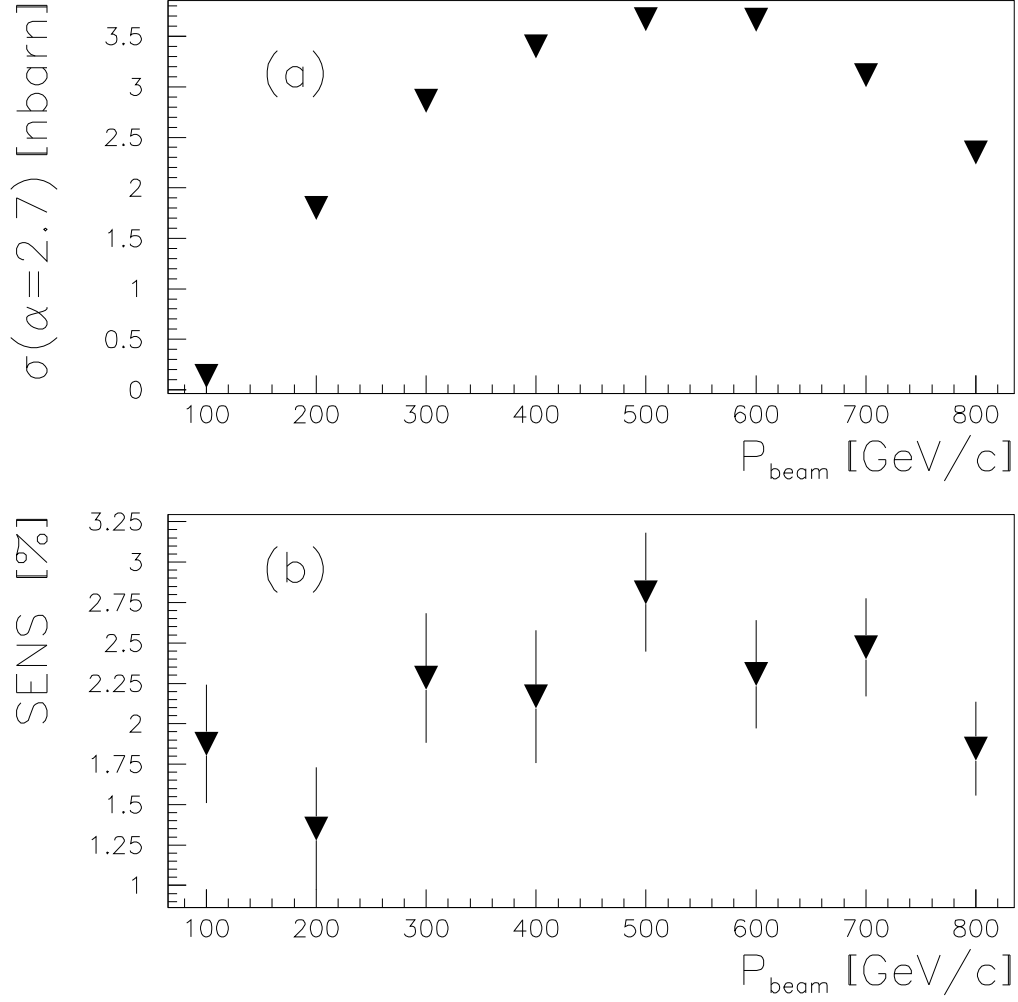


FIG. 13. (a) Total cross section of pion VCS for $\bar{\alpha} = 2.7 \times 10^{-43} \text{ cm}^3$ as a function of the beam momentum including the requirements of Eq. (44); (b) $SENS$ distribution as a function of the beam momentum including the requirements of Eq. (44).

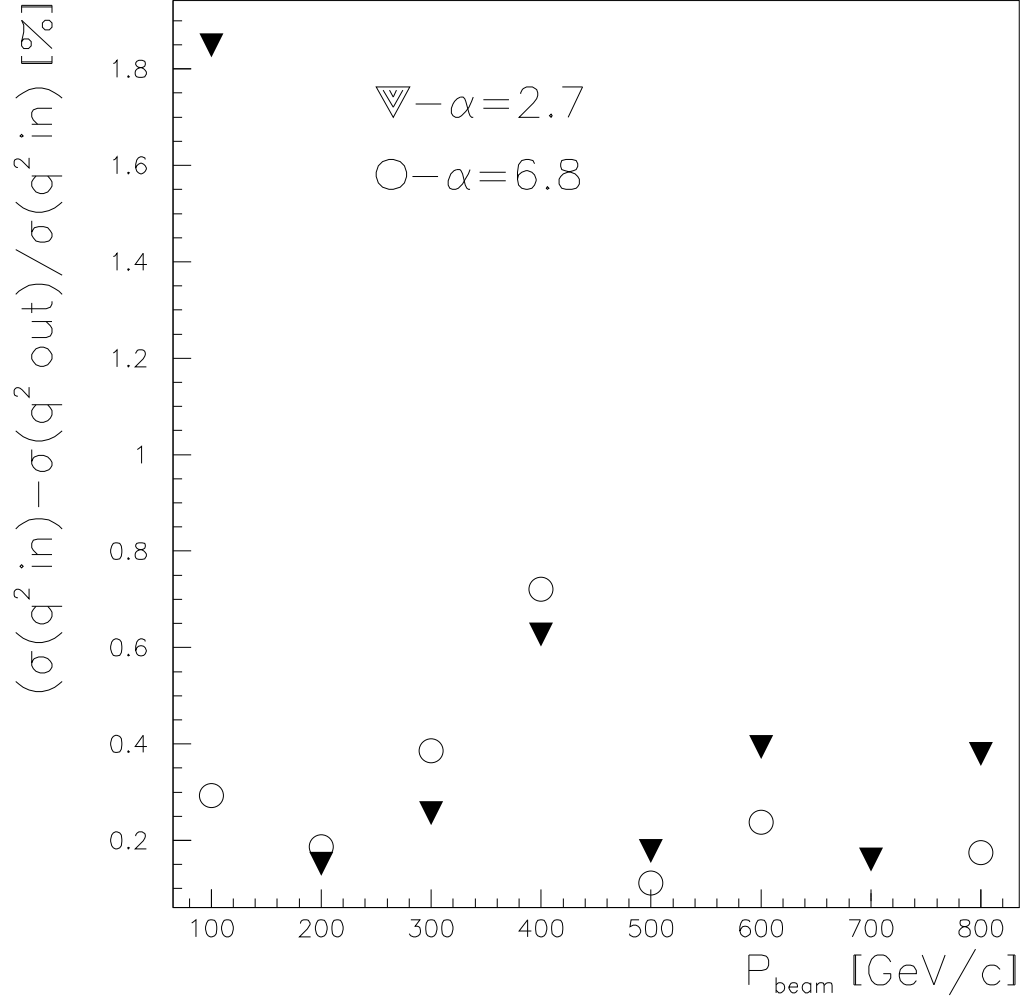


FIG. 14. Difference in the total (sensitive) cross section as a function of the beam momentum with and without q^2 dependence of \mathcal{M}_{NB} amplitude [see Eq. (25)] for $\bar{\alpha} = 2.7$ and $\bar{\alpha} = 6.8 \times 10^{-43} \text{ cm}^3$.

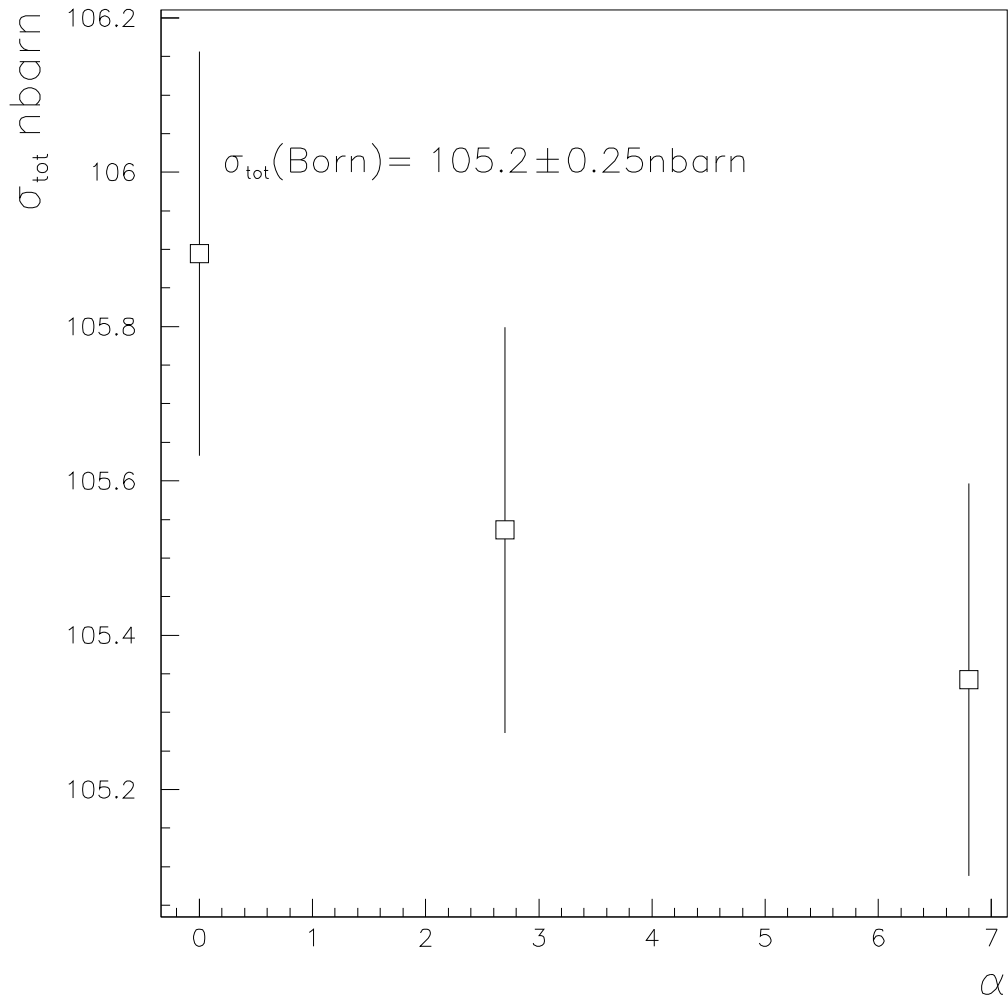


FIG. 15. Total cross section of $\pi^- e \rightarrow \pi^- e \gamma$ as a function of $\bar{\alpha}$. $\bar{\alpha}$ is given in units of 10^{-43} cm^3 .